

The VLT-FLAMES Tarantula Survey

XIV. The O-Type Stellar Content of 30 Doradus

N. R. Walborn¹, H. Sana^{1,2}, S. Simón-Díaz^{3,4}, J. Maíz Apellániz⁵, W. D. Taylor^{6,7}, C. J. Evans⁷, N. Markova⁸,
D. J. Lennon⁹, and A. de Koter^{2,10}

¹ Space Telescope Science Institute, 3700 San Martin Drive, Baltimore, MD 21218, USA

² Astronomical Institute Anton Pannekoek, University of Amsterdam, Kruislaan 403, 1098 SJ, Amsterdam, The Netherlands

³ Instituto de Astrofísica de Canarias, E-38200 La Laguna, Tenerife, Spain

⁴ Departamento de Astrofísica, Universidad de La Laguna, E-38205 La Laguna, Tenerife, Spain

⁵ Instituto de Astrofísica de Andalucía-CSIC, Glorieta de la Astronomía s/n, E-18008 Granada, Spain

⁶ Scottish Universities Physics Alliance, Institute for Astronomy, University of Edinburgh, Royal Observatory Edinburgh, Blackford Hill, Edinburgh, EH9 3HJ, UK

⁷ UK Astronomy Technology Centre, Royal Observatory Edinburgh, Blackford Hill, Edinburgh EH9 3HJ, UK

⁸ Institute of Astronomy, National Astronomical Observatory, Bulgarian Academy of Sciences, PO Box 136, 4700 Smoljan, Bulgaria

⁹ European Space Agency, European Space Astronomy Centre, Camino Bajo del Castillo s/n, Urbanización Villafraanca del Castillo, E-28691 Villanueva de la Cañada, Madrid, Spain

¹⁰ Instituut voor Sterrenkunde, KU Leuven, Celestijnenlaan 200D, 3001 Leuven, Belgium

ABSTRACT

Detailed spectral classifications are presented for 352 O–B0 stars in the VLT-FLAMES Tarantula Survey ESO Large Programme, of which 213 O-type are judged of sufficiently high quality for further morphological analysis. Among them, six subcategories of special interest are distinguished. (1) Several new examples of the earliest spectral types O2–O3 have been found, while a previously known example has been determined to belong to the nitrogen-rich ON2 class. (2) A group of extremely rapidly rotating main-sequence objects has been isolated, including the largest $v \sin i$ values known, the spatial and radial-velocity distributions of which suggest ejection from the two principal ionizing clusters NGC 2070 and NGC 2060. (3) Several new examples of the evolved, rapidly rotating Onfp class show similar evidence, although at least some of them are spectroscopic binaries. (4) No fewer than 48 members of the Vz category, hypothesized to be on or near the zero-age main sequence, are found in this sample; in contrast to the rapid rotators, they are strongly concentrated to the ionizing clusters and a newly recognized region of current and recent star formation to the north, supporting their interpretation as very young objects, as do their relatively faint absolute magnitudes. (5) A surprisingly large fraction of the main-sequence spectra belong to the recently recognized V((fc)) class, with C III emission lines of similar strength to the usual N III in V((f)) spectra, although a comparable number of the latter are also present, as well as six objects with very high-quality data but no trace of either emission feature, presenting new challenges to physical interpretations. (6) Two mid-O Vz and three late-O giant/supergiant spectra with morphologically enhanced nitrogen lines have been detected. Absolute visual magnitudes have been derived for each star with individual extinction laws, and composite Hertzsprung-Russell Diagrams provide evidence of the multiple generations present in this field. Spectroscopic binaries, resolved visual multiples, and possible associations with X-ray sources are noted. Astrophysical and dynamical analyses of this unique dataset underway will provide new insights into the evolution of massive stars and starburst clusters.

Key words. Galaxies: star clusters: individual: 30 Doradus – Magellanic Clouds – Stars: early-type – Stars: fundamental parameters – Stars: massive – Stars: spectral classification

1. Introduction

30 Doradus in the Large Magellanic Cloud (LMC) comprises the most massive starburst cluster and giant H II region in the Local Group, and it contains the most massive stars known (Crowther et al. 2010; Bestenlehner et al. 2011). It is the paradigm for understanding early massive stellar and cluster evolution, and for interpreting more distant starbursts. Thus it is appropriate that 30 Dor is the subject of the unprecedented spectroscopic dataset obtained by the VLT-FLAMES Tarantula Survey (VFTS; ESO Large Programme 182.D-0222; Evans et al. 2011), which contains high-resolution ($R \sim 10^4$) observations of about 800 OB stars in this field. Of these, 352 from the Medusa-Giraffe multi-object spectrograph configuration have been determined to be of

spectral type O (or B0 in 10 cases included here) and are the subject of this morphological investigation.

The prior state of the art in digital spectral classification of the O stars is represented by the Galactic O-Star Spectroscopic Survey (GOSSS; Maíz Apellániz et al. 2011; Sota et al. 2011), in which the system and procedures have been further developed and refined. An expanded list of standard stars and an extensive new classification atlas from those high-S/N data are presented there; many of the GOSSS developments have been applied in the present work. However, the resolution of the VFTS data is substantially higher, which has required additional developments and another new atlas of primarily Galactic spectra, from the IACOB survey (Simón-Díaz et al. 2011) in the northern hemisphere and the ESO archives in the southern, as discussed in detail and presented by Sana et al. (2014a, in prep.). Most of that

discussion will not be repeated here, but it was determined that $R \sim 4000$ is the practical upper limit for reliable visual spectral classification of O-type spectra, because of the effects of line-profile differences and numerous weak lines at higher resolving powers, so that value has been adopted for the new atlas and for this work.

Section 2 provides some further details about the data and classification procedures used here, including the specification of the high-quality subset of 213 objects isolated for further analysis, based on not only data characteristics but also multiplicity considerations. Experience has shown that substantial advances in data quality and/or sample size generally produce both foreseeable and unexpected new scientific results; the present study is no exception, and Section 3 describes six spectroscopic categories of special interest encountered among this subsample, some previously recognized (with new members added here) but others newly distinguished. Section 4 references the essential, tailored extinction corrections required for astrophysical analysis in regions of this kind and presents empirical and theoretical Hertzsprung-Russell Diagrams (HRDs) for the high-quality subsample. Possible associations with *Chandra* X-ray sources (Townsend et al. 2006) are noted in Section 5. Section 6 provides a summary, conclusions, and outlook for further analyses of these data by the VFTS Team.

2. Data and Analysis

Full details of the instrumental parameters and data reductions were provided by Evans et al. (2011). In brief, the VFTS data discussed here were obtained with the Medusa-Giraffe mode of the Fibre Large Array Multi-Element Spectrograph (FLAMES) instrument (Pasquini et al. 2002) at the Very Large Telescope (VLT) on Cerro Paranal, Chile. Each target was observed with the standard LR02 and LR03 settings of the Giraffe spectrograph (providing coverage of 3960–5071 Å at R of 7000–8500). At least six observations were obtained with the LR02 setting to support the investigation of spectroscopic binaries (Sana et al. 2013). Most of the observations were done during 2008 October through 2009 February, with a final epoch in 2009 October to extend the binary period sensitivity.

The LR02 and LR03 observations were coadded to produce the spectrograms studied here, so data below and above ~ 4500 Å correspond to different observations/epochs. Thus, in a rare, unlucky case of spectral variability, it is possible that an unreal spectrum has been synthesized. However, the individual observations were each inspected, and those of lower quality or subject to apparent artifacts were omitted from the sums. Most real variations correspond to either SB2 or SB1 systems; the former have been treated separately as further discussed below, while the latter were shifted for coaddition. Further processing steps undertaken for this work were rectification and rebinning to $R \sim 4000$, prior to plotting each spectrogram with a large scale matching that of the Sana et al. (2014a, in prep.) atlas for visual classification.

Among other refinements in GOSSS (Sota et al. 2011), the late-O/early-B spectral types and standards were redefined to maintain constant He line ionization ratios at all luminosity classes, in order to improve the consistency and reliability of the results. To this end, the O9.7 spectral subclass was introduced at the lower luminosity classes (V through III) for the first time, and some previous standards were shifted to the adjacent earlier subclasses. As also discussed by Sana et al. (2014a, in prep.), during the present work a further development along these lines

Table 1. Spectral-Type Distribution of AAA-Rated Classifications for VFTS O Stars

SpT	No.
O2	7
O3	11
O4	12
O5	11
O6	27
O7	24
O8	14
O8.5	17
O9	21
O9.2	8
O9.5	42
O9.7	19

was found to be warranted and useful, namely the introduction of the new subclass O9.2 to describe spectra with the He II lines ($\lambda\lambda 4541, 4200$) in the relevant ratio criteria just slightly weaker than the respective He I lines ($\lambda\lambda 4387, 4144$). The range in these ratios at O9.5 appeared excessive and the number of VFTS objects placed in that subclass is larger than in any other (Table 1). Thus, O9.2 is symmetrical with respect to O8.5, in which the same He II lines are slightly stronger than the He I, i.e., these ionization ratios are inverted between those two subclasses, on opposite sides of the unit ratios at O9. A sequence of these spectral types selected from the VFTS data is shown in Figure 1¹.

The present spectral classifications of the 213 most highly rated (AAA) VFTS O-type data are listed in Table 2, and their spatial distribution in the 30 Doradus field is shown in Figure 2. Their positions are given by VFTS identification number in Evans et al. (2011) and are not reproduced here, although their *BV* photometry is. Absolute visual magnitudes, effective temperatures, and bolometric luminosities derived here as referenced later are also listed. Spectroscopic and visual multiplicity information is given, as are cross-identifications with previous work to facilitate comparisons and recognition of new discoveries of special interest here. The remaining 139 (BBB) VFTS O–B0 classifications are listed in Appendix A, along with the various reasons for their lower ratings and discussion of some of them.

The visual spectral classifications presented here for the apparently constant-velocity and (shifted) SB1 objects have been performed on large-scale paper plots. The GOSSS classifications are being done with an electronic standard-spectra comparator (MGB; Maíz Apellániz et al. 2012). That program also supports the simultaneous classification of double-lined spectra, which has been carried out for the SB2 in the present sample by JMA; these results are included in the BBB list here, pending more detailed analysis of the separate components.

¹ It must be noted that there is a N III feature blended with He II at 4200 Å with the present resolution, which may affect the appearance of the relevant He ionization ratio when the He II is weak, i.e., at late-O types. Such an effect would be most pronounced in supergiant spectra, in which the N III lines are normally enhanced, or in N-enhanced spectra at any luminosity class. Indeed, there are some spectra in which these two He ionization ratios appear somewhat discrepant, frequently in the sense that $\lambda 4200/\lambda 4144$ is greater than $\lambda 4541/\lambda 4387$, which may well be due to the N III contribution at $\lambda 4200$. Clarification of this issue will require higher resolution and/or spectral synthesis.

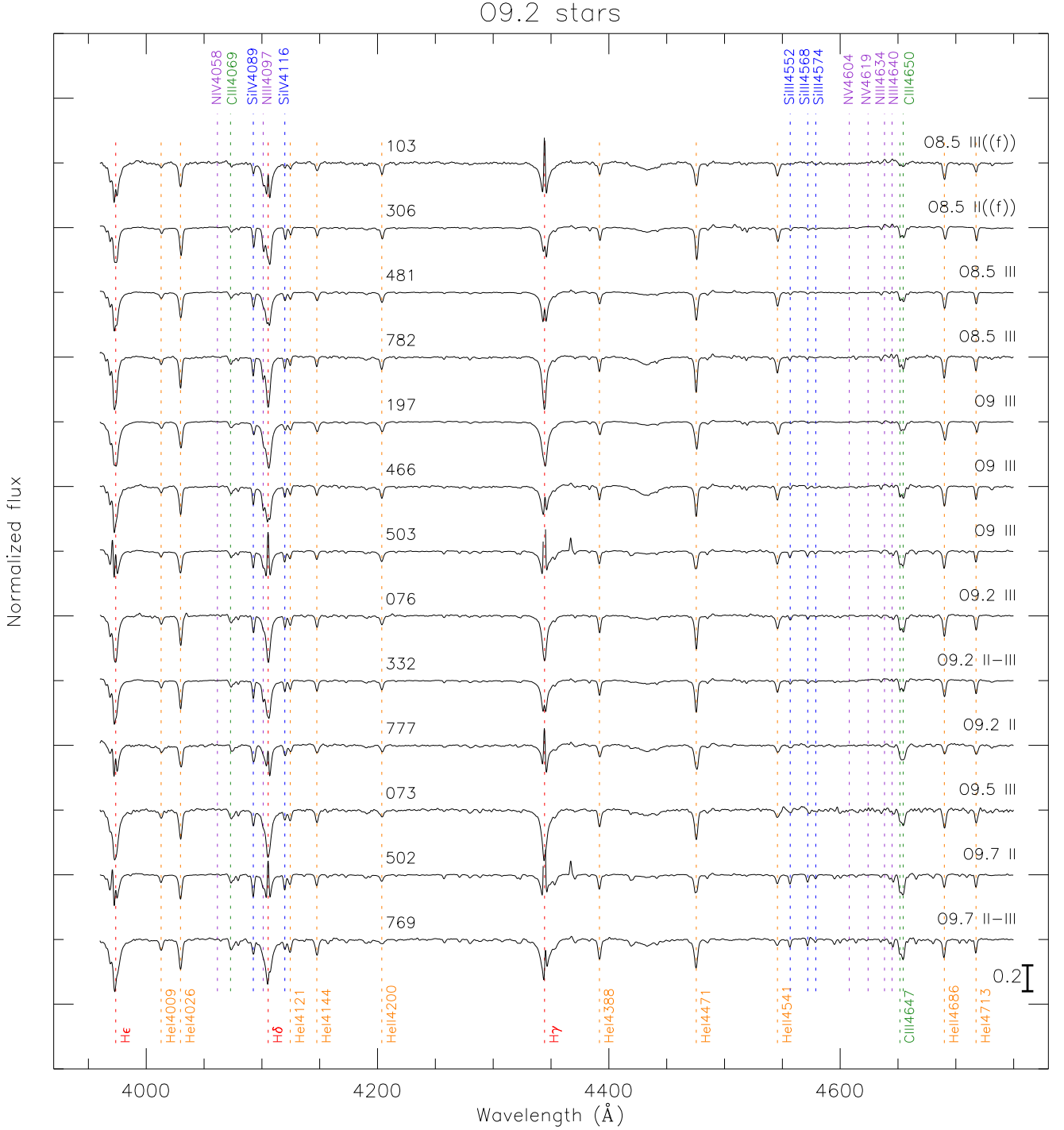


Fig. 1. A sequence of O8.5 through O9.7 spectra from the VFTS sample, to illustrate the new O9.2 type in terms of the He II $\lambda\lambda 4541, 4200$ /He I $\lambda\lambda 4387, 4144$ and He II $\lambda 4541$ /Si III $\lambda 4552$ criteria. $\lambda 4026$ is a blend of He I and He II, with the former predominating at late-O types. The ordinate scales in all spectroscopic figures are given in continuum units by the bar at lower right. These figures should be viewed online with at least 200% enlargement to fully appreciate their information content.

3. Special Spectroscopic Categories

The VFTS ID numbers of several special categories of O-type spectra in 30 Doradus are listed in Table 3. The spectra and spatial distributions of most of these categories are presented and discussed in turn in this section; note that many objects are in more than one. The SB? category consists of spectra that exhibit radial-velocity displacements between the stellar absorption and

nebular emission lines, but in which significant radial-velocity variations have not been detected. The Galactic SB 9 Sagittarii has a period of 8.6 yrs (Rauw et al. 2012) and would likely display little motion during the interval of the initial VFTS observations. While most of the SB? are likely SB, the alternative explanation of anomalous stellar or nebular motions cannot be excluded a priori.

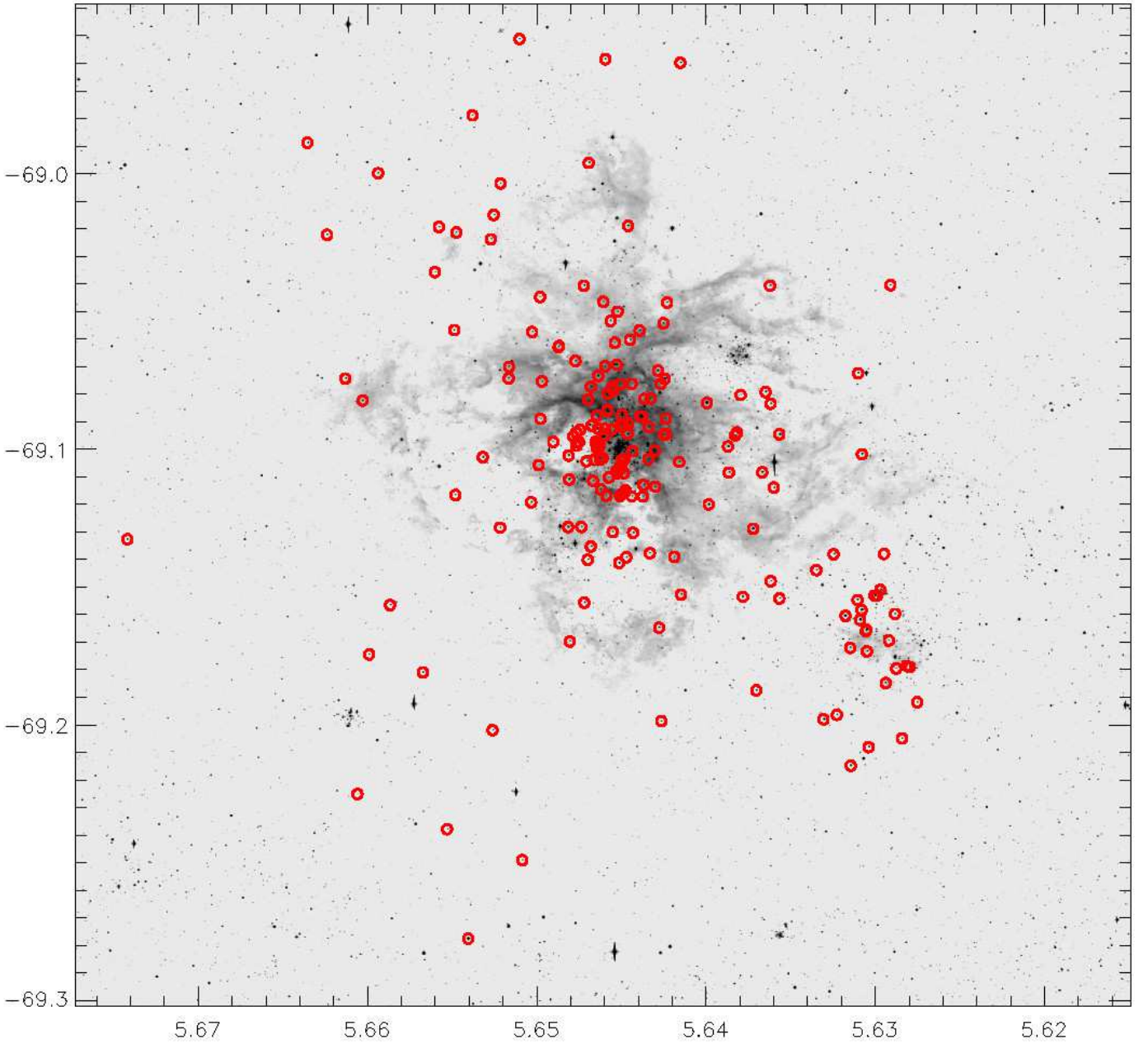


Fig. 2. Locations of the 213 AAA O stars in the 30 Dor field, represented by a visual image from the ESO 2.2 meter Wide Field Imager. The axes are labeled with equatorial coordinates in hours of right ascension and degrees of declination in this and all subsequent direct images. NGC 2070 (including R136, the bright object above center) is the ionizing cluster of the Tarantula Nebula, while NGC 2060 is a somewhat older association 6' (90 pc in projection) to the SW.

3.1. O2-O3 Stars

The classification of the hottest Population I spectra was discussed by Walborn et al. (2002a, 2004) and has been recently analyzed quantitatively by Rivero González et al. (2012a). 30 Doradus has been known for some time to contain the strongest resolved concentration of these extreme objects (Parker 1993; Walborn & Blades 1997; de Koter et al. 1997, 1998; Massey & Hunter 1998; Bosch et al. 1999). Our sample includes 18 stars of these spectral types (not including the intermediate Of*/WN objects discussed by Crowther & Walborn 2011), of which 9 (VFTS 16, 143, 267, 404, 512, 532, 621, 755, 797) are believed to be newly classified as such (cf. cross-identifications with earlier work in Table 2)—although all of the

present classifications are of higher quality and many are not identical to previous results for that reason. The VFTS blue-violet spectrograms of all these stars are shown in Figures 3 and 4, while their spatial distribution is in Figure 5.

Objects to be distinguished even among this exceptional group include the runaway star VFTS 16 (Evans et al. 2010). VFTS 72 = BI 253 is another runaway candidate based on its location (Fig. 5 here; Walborn et al. 2002a); in that reference it was adopted as a luminosity class V standard, but it is assigned V-III here, indicating either a data-quality effect or some variability.

VFTS 506 is newly recognized as a member of the surprising ON2 subtype introduced and discussed by Walborn et al. (2004). VFTS 169 has been classified O2.5 V(n)((f*)); the type

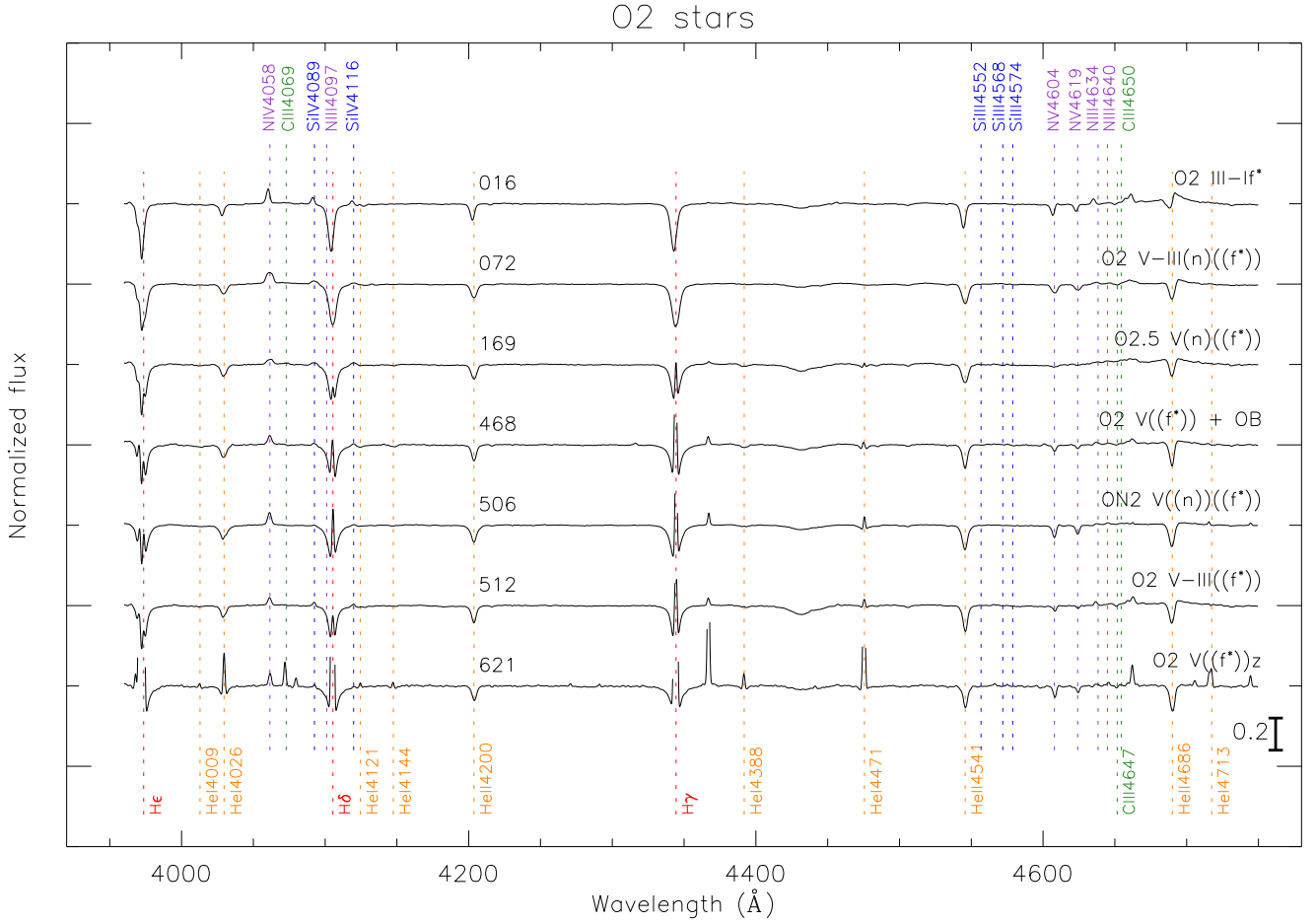


Fig. 3. VFTS spectra of type O2. $\lambda 4026$ is a blend of He I and He II, with the latter predominating at early-O types. C III $\lambda 4069$, 4650 and N III $\lambda 4640$ are blends, primarily with other lines from the same multiplets in O-type spectra. Strong nebular emission lines are truncated to avoid overlapping adjacent spectra.

corresponds to an interpolation of the N IV / N III emission-line ratio between O2 and O3. This object is not an exemplar of the type because of its weak, broad lines; published precedents are N11-26 (Evans et al. 2006) and HD 93162 (Crowther & Walborn 2011).

VFTS 566 and 599 are the first high-quality representatives of the O3 III(f*) spectral type, for which no clear example could be identified by Walborn et al. (2002a); VFTS 518 = P901 (Bosch et al. 1999) is a nice paradigm for O3.5 III(f*). VFTS 180 was originally classified as an intermediate Of*/WN type by Schild & Testor (1992) and hence appears in the LMC Wolf-Rayet (WR) catalogue (Breysacher et al. 1999); but in their detailed rediscussion of that category, Crowther & Walborn (2011) reclassify it as a pure Of* type.

VFTS 755 is a member of the extremely rapidly rotating dwarf category discussed in the next Section 3.2. VFTS 94 = ST1-28 is also a member of the Onfp category discussed in Section 3.3; it is definitely an SB but its double-lined status is uncertain, which is why it is included in the AAA list (rather than the BBB where most SB2 are found). VFTS 532 and 621 also belong to the Vz category (Section 3.4). VFTS 143, 404, and 797 are also in the V((fc)) category (Section 3.5); the first two are large-amplitude SB1 and the third a possible SB.

3.2. Extreme Rotator Runaways

Perhaps the most striking and unexpected result of this investigation is described in this subsection. It consists of the discovery of a category of 18 extremely rapid rotators (Figure 6), including the fastest known, whose peripheral space distribution with respect to the ionizing clusters (Figure 7) immediately suggests a runaway nature. This interpretation is already supported by their peculiar radial-velocity distribution, with a high fraction of large relative values (Sana et al. 2012; Sana et al. 2014b, in prep.). The average projected distance from R136 of the 13 of them within 81 pc is 40 ± 7 (error of the mean, hereafter m.e.) pc. For comparison with the distribution of the Vz stars as discussed in Section 3.4 below, their average separation in RA from R136 (i.e., from the NS axis of the Tarantula) is 30 ± 5 (m.e.) pc. Remarkably, the projected distances from R136 of VFTS 722 and 724, which have identical spectral types but are located at opposite NS extremes of the field, are both 132 pc; moreover, both have peculiar radial velocities on opposite sides of the cluster mean.

Figures 7 and 8 also display a number of moderate (projected) rotators in the same peripheral areas, for further investigation as *hypothetical* very rapid rotators with high axial inclinations. Two of them, VFTS 356 and 761, do have high peculiar radial velocities consistent with a runaway nature (Sana et al.

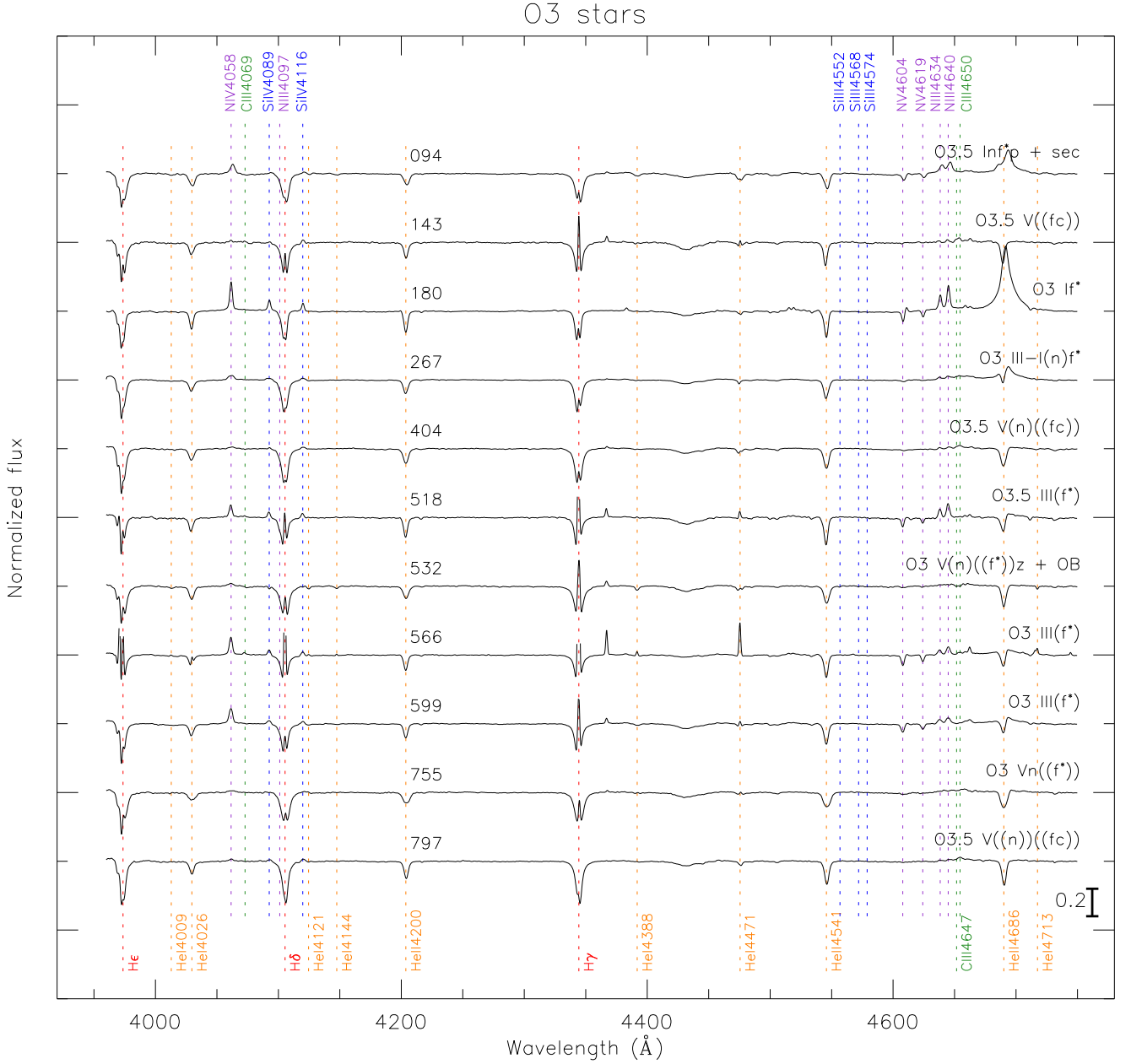


Fig. 4. VFTS spectra of type O3.

2014b, in prep.), while three more, VFTS 250, 355, and 797, have moderately anomalous values.

The projected equatorial rotational velocities (Ramírez-Agudelo et al. 2013 and this paper) together with the radial velocities (Sana et al. 2013) of both the high and these selected moderate rotators are displayed graphically in Figure 9, which also shows the progression of the line-broadening classification n -parameter and its high degree of correspondence with the $v \sin i$ values. Technical details and uncertainties of the $v \sin i$ derivations can be found in Ramírez-Agudelo et al. (2013); as discussed there and by Simón-Díaz & Herrero (2014), the effect of macroturbulence is essentially negligible for $v \sin i > 120 \text{ km s}^{-1}$, i.e., the range of interest here. Other potential effects, such as that of gravity darkening in very rapid rotators, will be addressed in future VFTS investigations of the rotational velocities.

The objects in the field image (Fig. 7) are all of luminosity class V, but Figures 9 and 10 also display several extreme rotators classified as late-O giants, for further consideration of their actual luminosities. E.g., if the He II $\lambda 4686$ absorption line were filled in by emission due to some cause other than higher luminosity in these extreme objects, they could have lower actual luminosities; and the luminosity classes of two of them are flagged as uncertain. In fact, the average M_V of 4 late-O V and 5 late-O III rapid rotators with determinations in Table 2 are indistinguishable at -3.85 ± 0.07 , compared to calibration values of -4.2 for the former and -5.45 for the latter (Walborn 1973), indicating that all of them are actually dwarfs, as further discussed later. VFTS 399 is an extreme X-ray flare object, as mentioned in Section 5.

The previously most rapidly rotating O stars known were recently discussed by Walborn et al. (2011), with highest $v \sin i$

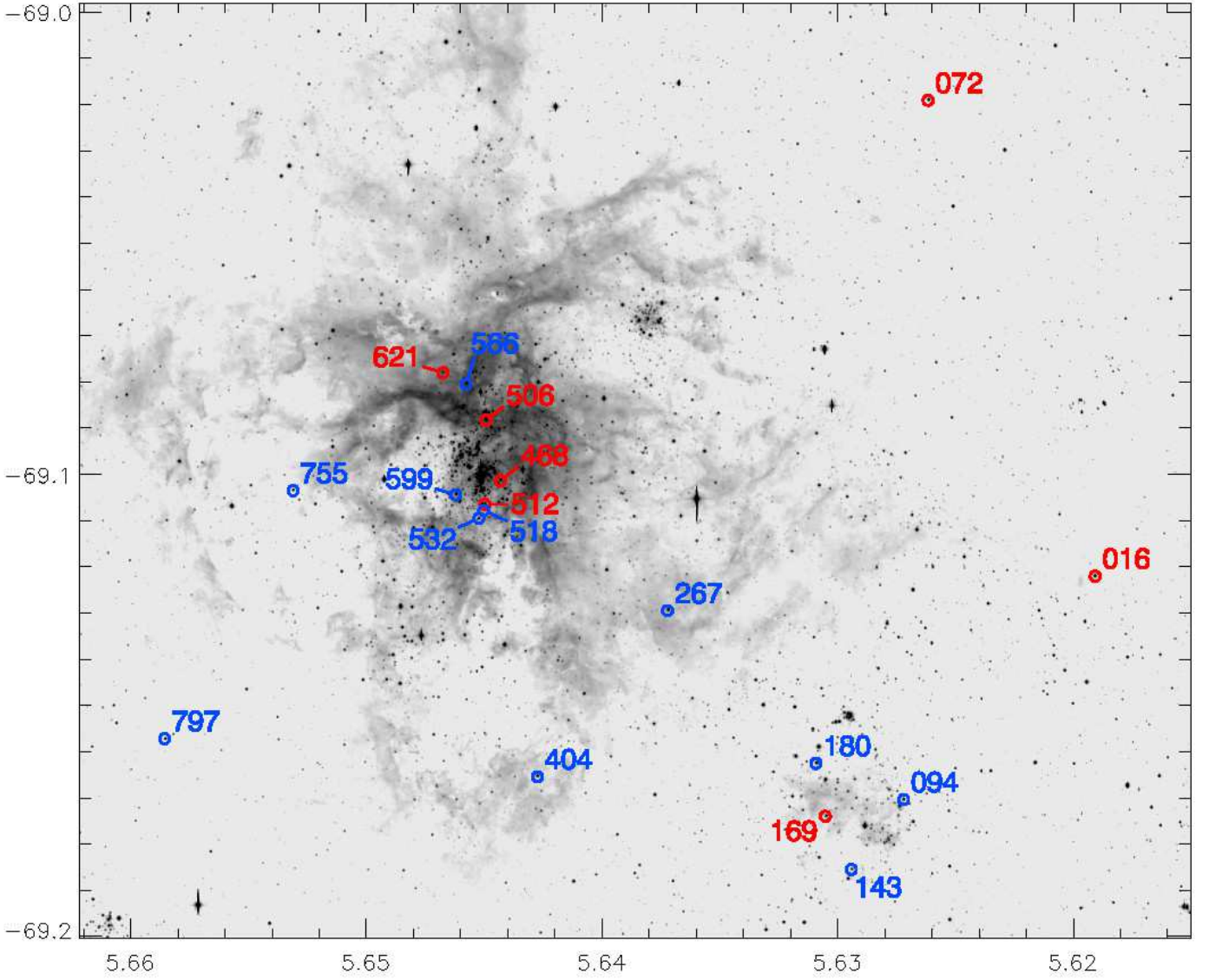


Fig. 5. Spatial distributions of the O2 (red) and O3 (blue) stars.

values somewhat exceeding 400 km s^{-1} . Two objects in the VFTS 30 Dor sample surpass them substantially, with values $\sim 600 \text{ km s}^{-1}$. The first to be discovered and assigned the nnn qualifier was VFTS 285 (Walborn et al. 2012), which has very high-S/N data (Fig. 6). The other, VFTS 102, has lower quality data with a somewhat uncertain spectral type and is hence in the present BBB list (Appendix A); this object and its possible association with the X-ray pulsar PSR J0537-6910 are discussed separately by Dufton et al. (2011).

Remarkably, none of these stars (except VFTS 102) shows evidence of disk emission lines, even at $H\alpha$ (also covered by VFTS albeit not discussed here). VFTS 190 is a weak but definite member of the Onfp category discussed in the next Section 3.3, with weak emission wings at $\text{He II } \lambda 4686$ (Fig. 6), and it is a possible SB as many members of that category are. VFTS 406 was originally thought to be a pronounced member of that category but it was subsequently realized that its apparent emission features are due to contamination on the detector from the adjacent WN spectrum of R135, so it is included here as a normal extremely broad-lined dwarf.

The moderate (projected) rotator VFTS 72 is of type O2, while 404 and 797 are O3.5. As already noted in the previous section, the O3 type of VFTS 755 is the earliest among the extreme rotators. VFTS 184, 355, 356, 706, 722, 724, 751, and 761 are also members of the Vz category believed to be indicative of extreme youth (Section 3.4).

A significant population of high-mass, extreme rotators ejected from a massive young cluster is a new observational phenomenon. A current *HST* imaging program (PI DJL) will measure the proper motions of these stars if they are high, enabling a full kinematical analysis. Of course, the origins and destinies of these objects are of considerable interest. Spin-up by mass transfer in binaries (Langer et al. 2008) and ejection by dynamical processes in dense young clusters (Fujii & Portegies Zwart 2011) are strong hypotheses. There is evidence for a runaway nature of some gamma-ray burst progenitors, which should also be rapid rotators (Dale & Davies 2006; Allison et al. 2010). A possibly related phenomenon in the Galactic cluster Westerlund 2 has recently been discussed by Roman-Lopes et al. (2011).

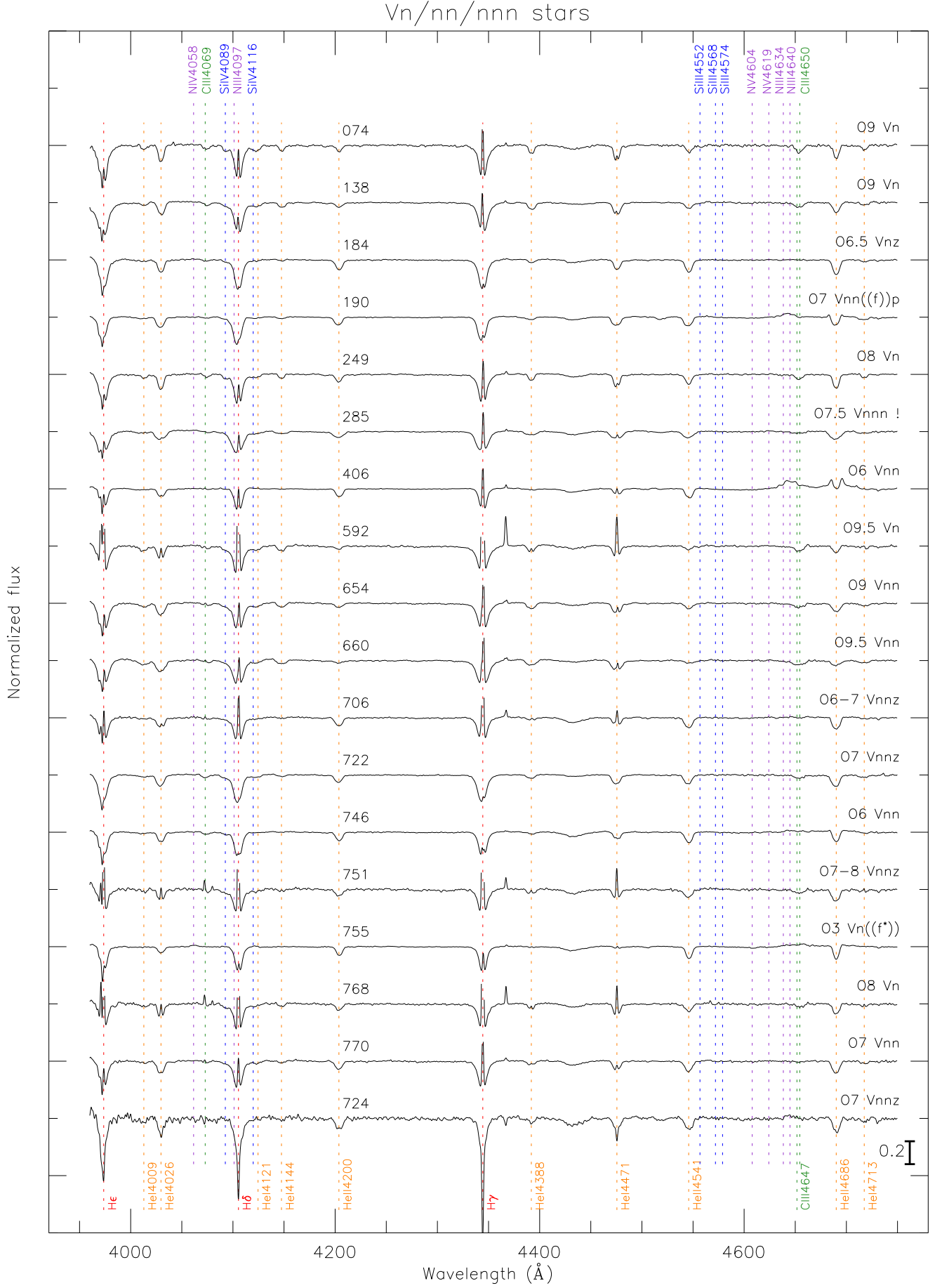


Fig. 6. VFTS spectra of very rapidly rotating luminosity class V stars. VFTS 285 is the most rapidly rotating O star known (the exclamation mark is not part of the spectral type!). VFTS 406 is contaminated by a nearby emission-line spectrum on the detector, i.e., the apparent N III and He II emission features are spurious. Note that VFTS 724 is out of the ID sequence because of the oversubtracted nebular emission lines.

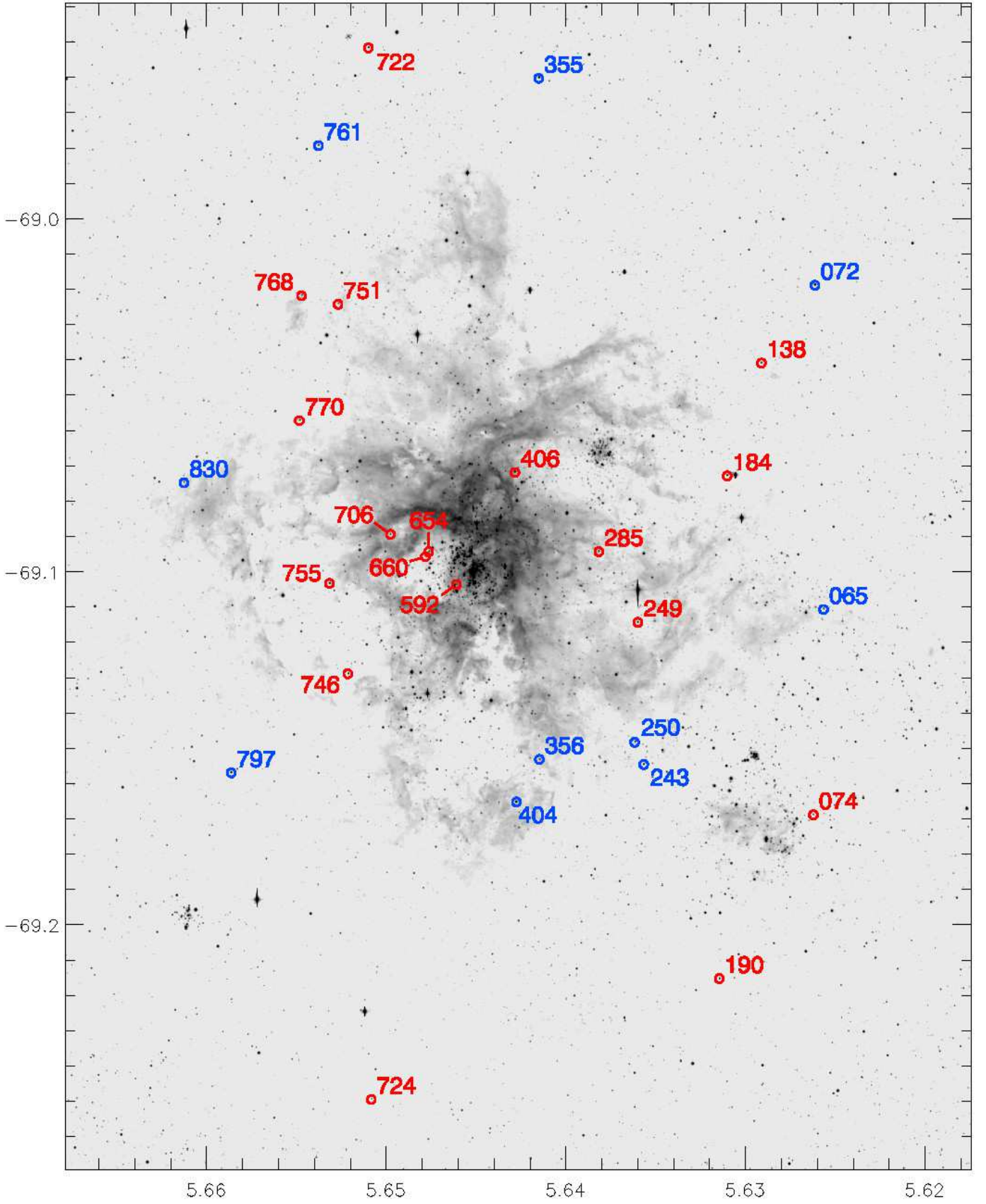


Fig. 7. Spatial distribution of the VFTS luminosity class V extreme rotators (red), and a selection of peripheral moderate (projected) rotators (blue).

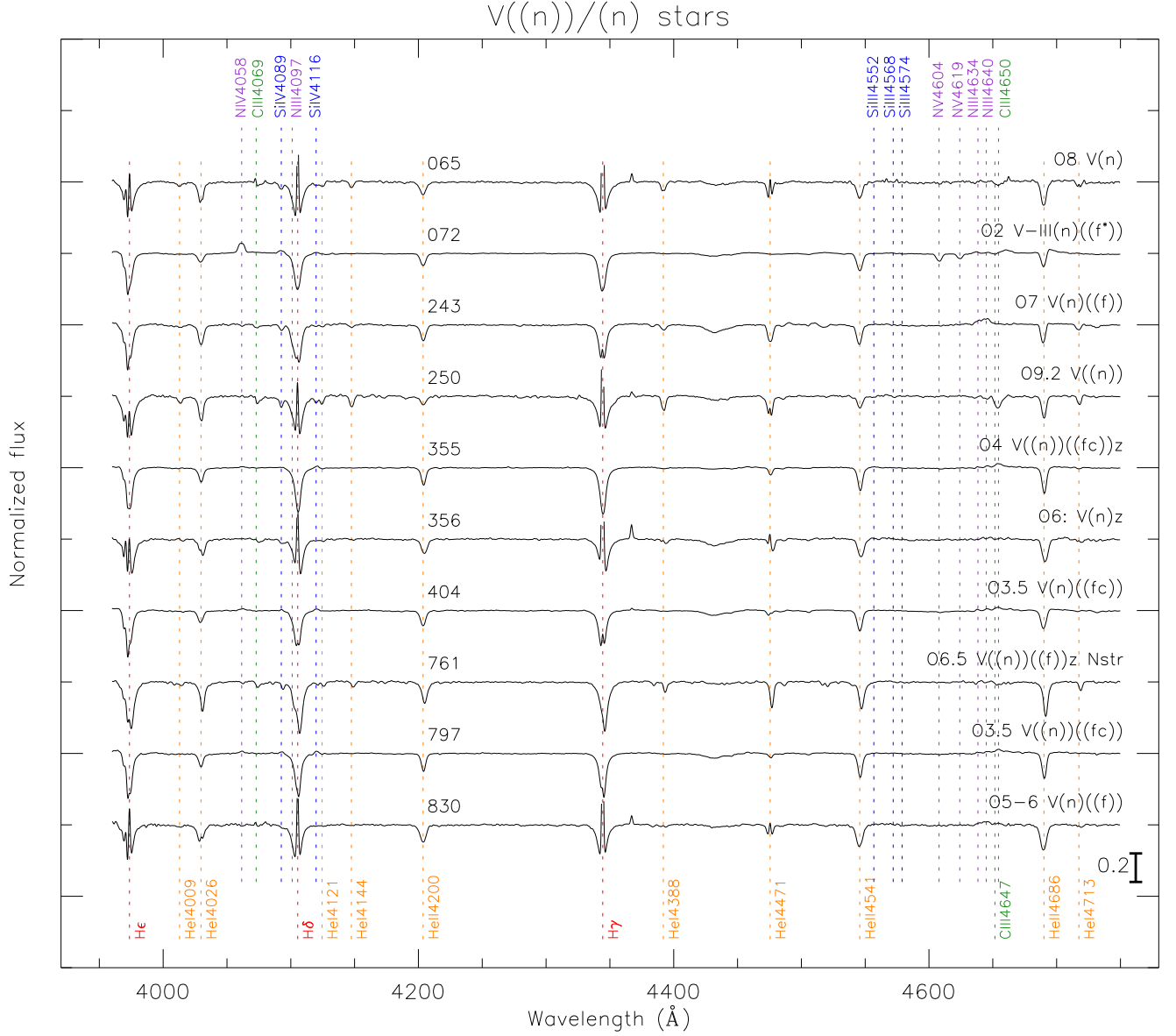


Fig. 8. VFTS spectra of selected peripheral moderate (projected) rotators.

3.3. Onfp Spectra

This peculiar category of rapid rotators with centrally reversed He II $\lambda 4686$ emission features was recently discussed by Walborn et al. (2010a), and its defining composite line profiles have been modeled in terms of rotating, clumped winds by Hillier et al. (2012). The VFTS sample includes 7 members of the class (Figure 11), 5 of which are new. Although the number is small, their spatial distribution (Figure 12) also suggests a runaway nature, which is a property of several previously known members elsewhere. There is growing evidence for a high fraction of binaries among them, while other apparently single objects have been suggested as possible mergers; spin-up by mass transfer and merging in binary systems could explain their current rapid rotation despite strong stellar winds, which would otherwise be expected to have braked these evolved objects.

VFTS 94 = ST1-28 and VFTS 208 = ST1-93 are spectroscopic binaries and spectrum variables associated with NGC 2060, as illustrated and discussed by Walborn et al.

(2010a). The period of VFTS 94 is 2.35 d while that of VFTS 208 has not yet been determined. VFTS 177 is far from the ionizing clusters and thus a runaway candidate (Fig. 12). VFTS 190 is a possible SB and also a candidate runaway from NGC 2060 (Figs. 11 and 12). VFTS 526 = P925 is a large-amplitude SB1; note the essential confirmation here of the basic spectral type derived from low-S/N data by Walborn & Blades (1997). VFTS 626 is another possible SB; this star and VFTS 526 are likely members of the R143 association rather than runaways (Walborn & Blades 1997). VFTS 656 is yet another large-amplitude SB1. The preponderance of binaries among these objects is consistent with prior results for the class.

As noted in the previous section, VFTS 406 was initially classified as a pronounced Onfp object, but the apparent characteristics of the class in this case were subsequently determined to be due to contamination by an adjacent WN spectrum on the detector. The resemblance of the contaminated spectrum to some Onfp types is remarkable (Fig. 6). Clearly one must be alert to this insidious effect in multiobject data. Also, some real Onfp

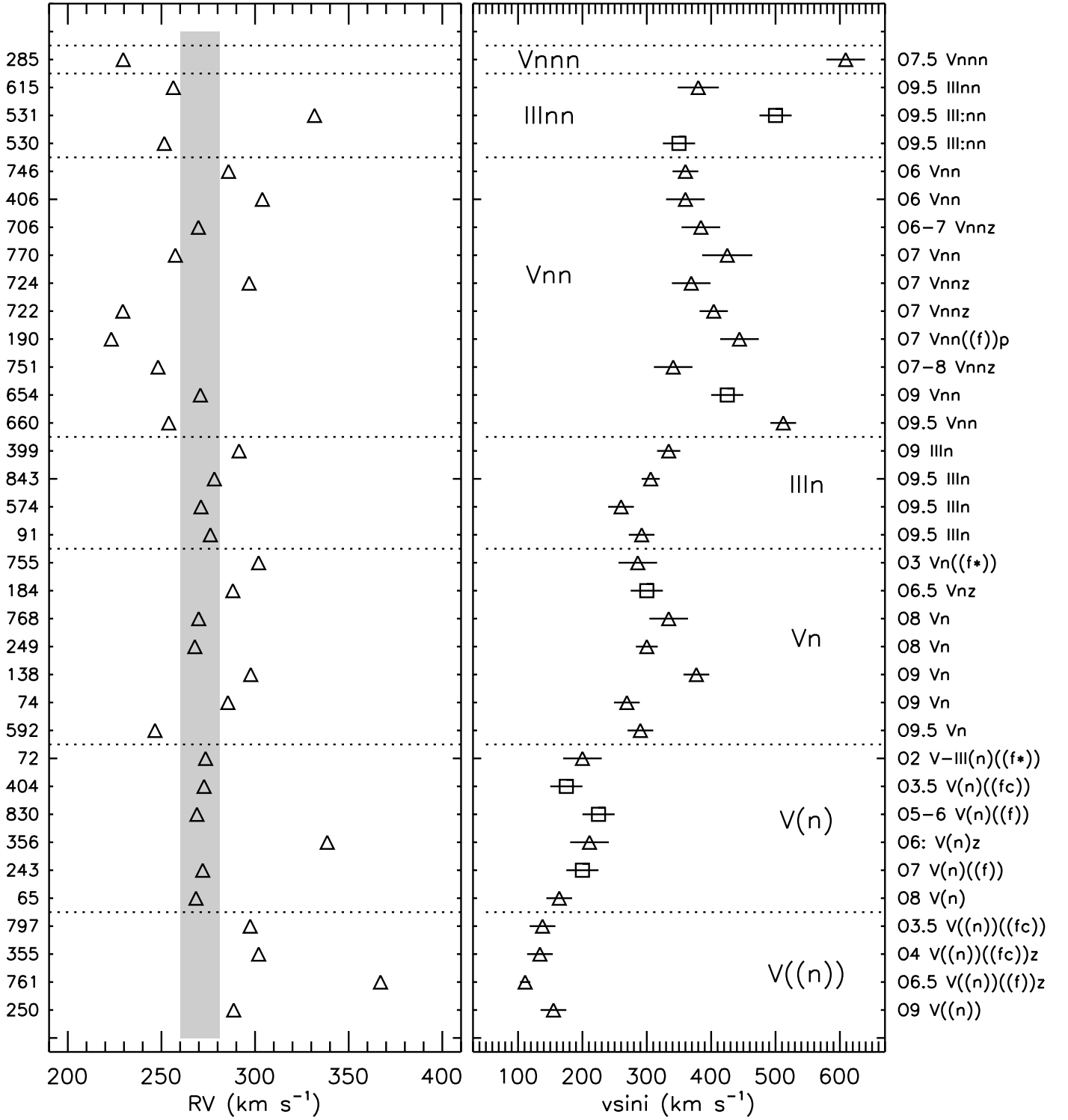


Fig. 9. Moderate to extreme rotators, grouped from bottom to top first by line-broadening parameter, then by luminosity class, and finally inversely by spectral subclass within each of the former parameters. VFTS numbers are given on the left vertical axis and the full spectral types on the right. Left panel: radial velocities from Sana et al. (2013) relative to the cluster means (vertical bar). Right panel: projected rotational velocities determined mostly by Ramírez-Agudelo et al. (2013) but some by SSD for this paper with similar techniques; squares indicate SB1 not included in the former reference and bars denote the uncertainties.

spectra could arise from analogous composite effects in binary systems, possibly including colliding-wind regions as found in the case of the Galactic star HD 152248 by Sana et al. (2001).

3.4. ZAMS Candidates

The defining characteristic of the Vz class, reviewed by Walborn (2009), is an He II $\lambda 4686$ absorption feature stronger than any other He line in the blue-violet region. Since emission filling in that line, namely the Of effect, has been established as a luminos-

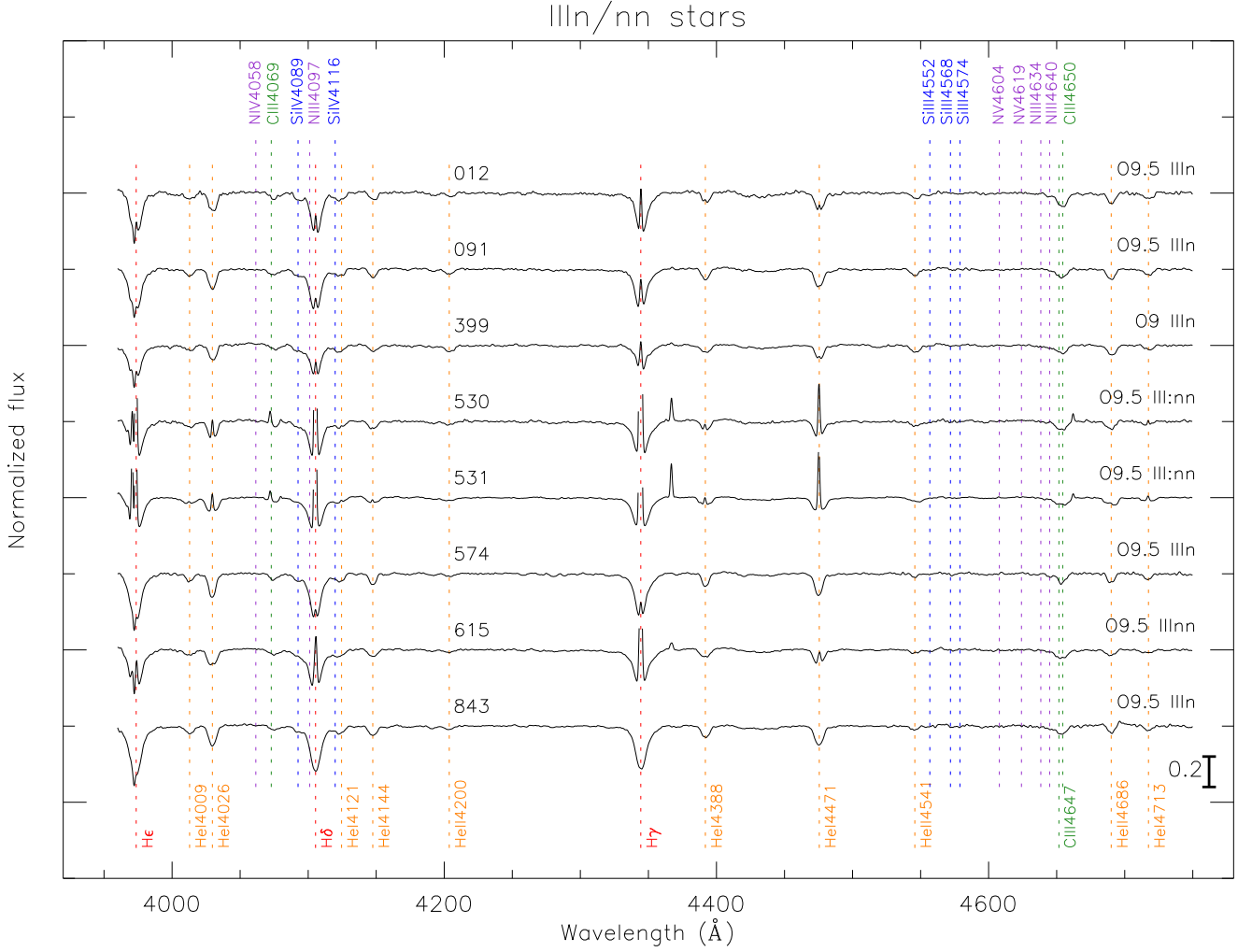


Fig. 10. VFTS spectra of very rapidly rotating late-O, luminosity class III stars.

ity indicator in normal O-type spectra, the Vz characteristic has been hypothesized as the inverse effect, i.e., less emission than in even normal class V spectra, corresponding to lower luminosity and extreme youth. Consistently with that hypothesis, Vz spectra are typically found in very young regions. Nevertheless, we were surprised to find no fewer than 48 such spectra among our 30 Dor AAA sample of 213 O stars (Figures 13–15).

Moreover, their spatial distribution appears essentially inverse to that of the rapid rotators, exhibiting a strong concentration toward the ionizing clusters NGC 2070 and 2060 (Figure 16). The average projected distance from R136 of 27 non-n/nn Vz stars within 81 pc is 27 ± 3 (m.e.) pc, which is not statistically very different from the result for the rapid rotators given in Section 3.2 above, despite the distinctly contrary impression from inspection of Figures 7 and 16. On further consideration, however, it is seen that the visual impression arises rather from the concentration of the Vz stars toward the NS axis of the elongated Tarantula nebula. Their average separation in RA from R136 (i.e., from the NS axis) is 9 ± 2 (m.e.) pc, which is indeed significantly different from the corresponding statistic for the rapid rotators (30 ± 5 (m.e.) pc).

In addition, there are a number of Vz objects in an east-west band at the northern edge of the nebula, coinciding with the locations of the WN stars R144, R146, and R147 (Feast et al. 1960)

as well as a compact H II region that is a highly luminous *Spitzer* source (Walborn et al. 2013); this northern 30 Dor region of recent and current star formation has been newly recognized in this work. The overall spatial morphology of the Vz objects in 30 Dor provides further evidence for the youth of most of them, i.e., a (near) zero-age main sequence (ZAMS) nature.

In the discussion of the rapid rotators in Section 3.2, it was noted that 8 of them are also in the Vz class, which at first appears to contradict the different spatial distributions of the two categories with respect to the nebula and ionizing clusters. However, by comparison of Figures 7 and 16, it can be seen that most of these stars lie at the boundaries of the two distributions, while a few belong to the northern Vz group. The potential extreme, opposite runaway nature of VFTS 722 and 724 was also discussed in Section 3.2.

It is noteworthy that two very underluminous O6.5 V((f))z stars, VFTS 089 ($M_V - 4.30$) and 761 ($M_V - 4.06$) have nitrogen-enhanced spectra. How this might come about in very young objects raises interesting possibilities, such as chemically homogeneous evolution or binary mass transfer. HD 12993 in the Galaxy is a similar case (Conti & Leep 1974; Walborn 1976; Sota et al. 2011). Further radial-velocity and quantitative analysis of these spectra may well provide important evolutionary insights (Rivero González et al. 2012b).

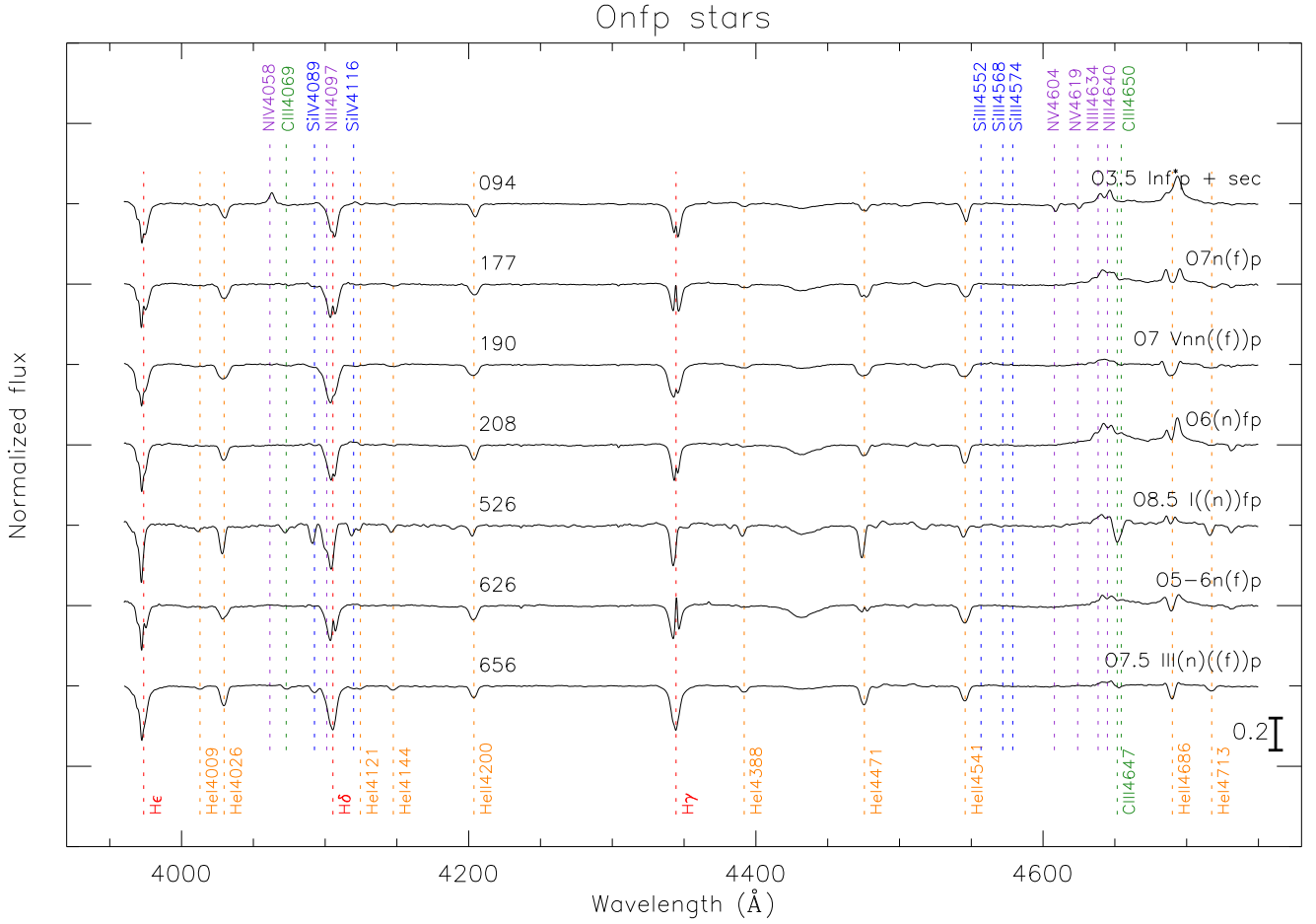


Fig. 11. VFTS Onfp spectra.

The high binary frequency of the O stars may provide an alternative origin for some Vz spectra: a composite of relatively early and late O-type normal dwarf spectra, in which the two components respectively dominate the He II and He I lines in the temperature-type classification ratios, while both contribute comparably to He II $\lambda 4686$, thus producing an apparent mid-O Vz morphology. Twenty-eight of the 48 Vz objects are definite or possible SB or visual multiples (Table 2). Some Galactic systems of this nature are currently under analysis within GOSSS and the associated high-resolution programs OWN (Barbá et al. 2010) and IACOB (Simón-Díaz et al. 2011).

Quantitative analyses of VFTS Vz spectra to investigate the hypothesis of smaller ages and lower luminosities have been carried out by Sabín-Sanjulián et al. (2014). Their results raise some further interesting questions about the class that will be discussed in the context of the absolute visual magnitudes and HRDs in Section 4 below. The Of effect is strongly related to the stellar winds. A key insight of the quantitative analysis is that, because the winds are weaker at lower metallicity, the Vz phenomenon may well be more frequent and have a greater duration in the LMC than in the Galaxy.

3.5. O V((fc)) and O III(fc) Spectra

A new category of O-type spectra that emerged from GOSSS was described by Walborn et al. (2010b). The defining characteristic is C III $\lambda\lambda 4647 - 4650 - 4652$ emission intensities com-

parable to those of the classical Of N III $\lambda\lambda 4634 - 4640 - 4642$ features. The new qualifier “fc” was introduced for this category, with the correlated progression of He II $\lambda 4686$ from strong absorption, through neutralized, to emission indicated by double, single, and no parentheses, respectively and analogously to the notation for “f” spectra. In the Galaxy, this phenomenon is peaked about spectral type O5 at all luminosity classes; in addition, there is a tendency for it to appear in certain clusters or associations but not others. Another surprise in the VFTS sample is the presence of 19 class V spectra with this characteristic (Figure 17), although their spectral-type range is broader than in the Galactic counterparts, and the C III emission tends to be *stronger* than the N III. Two Small Magellanic Cloud (SMC) objects with these characteristics were reported by Walborn et al. (2000); they were classified as OC partly on the basis of supporting evidence from the UV wind profiles, and of course the fc class did not yet exist. However, relationships to these VFTS objects and the lower metallicities in both galaxies are not excluded.

Two early O III(fc) spectra in the VFTS sample are shown in Figure 18, along with some O III(f) comparisons. It should also be noted that the primary component of the R139 = VFTS 527 SB2 system has a strong O6.5 Iafc spectrum (Taylor et al. 2011; Appendix A here).

Fourteen normal V((f)) spectra are likewise present in our sample (Table 3). Their spectra are shown in Figure 19, and the space distributions of these two luminosity class V subcategories

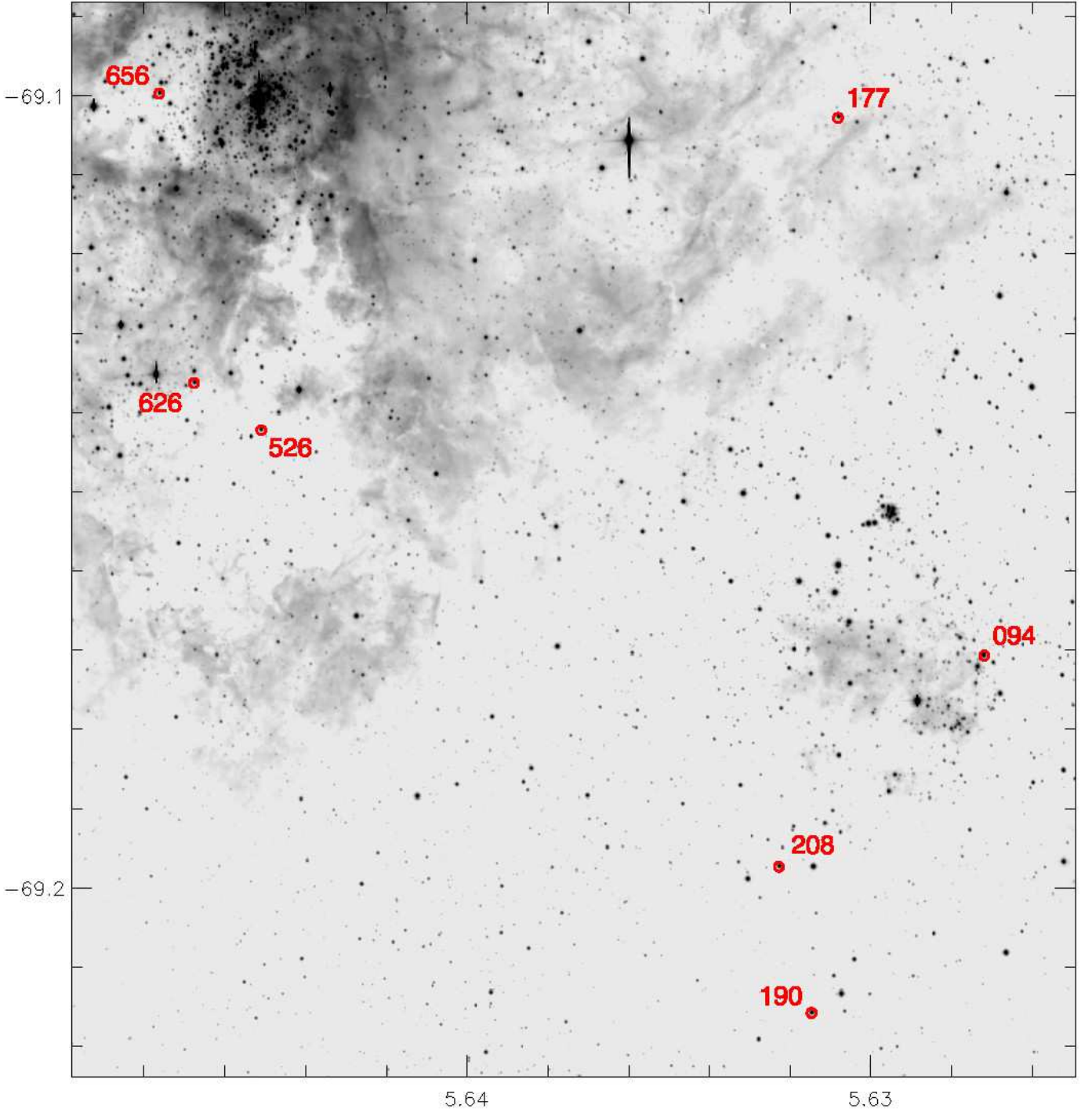


Fig. 12. Spatial distribution of Onfp stars.

are shown in Figure 20; they appear to be well mixed. Moreover, we have found six O V stars in our sample with very high-quality data but no trace of any emission lines (Table 3; Figure 21). Clearly these distinct variants of O main-sequence spectral morphology in 30 Doradus present interesting challenges for physical modeling, with significant structural and/or evolutionary insights likely to follow. The intricacies of N III and C III line formation in O-type spectra have recently been rediscussed by Rivero González et al. (2011) and Martins & Hillier (2012), respectively; it will be interesting to apply those results to detailed analysis of these spectra, to ascertain whether the model physics

is now adequate to explain them or not. As those papers emphasize, the effects of various parameters such as metallicity on these lines are far from straightforward.

As listed in Table 2, 14 of the 19 V((fc)), 7 of the 14 V((f)), and 1 of the 6 non-emission stars are definite or possible SB. There are also 11/19 V((fc)), 8/14 V((f)), and 5/6 V(no-emission) overlaps with the Vz, and some with other categories. These relationships should be taken into account in further analyses; at a minimum, they are obviously not excluded, and some of them may turn out to be significant beyond that basic fact. E.g., there appears to be a high fraction of SB among the V((fc));

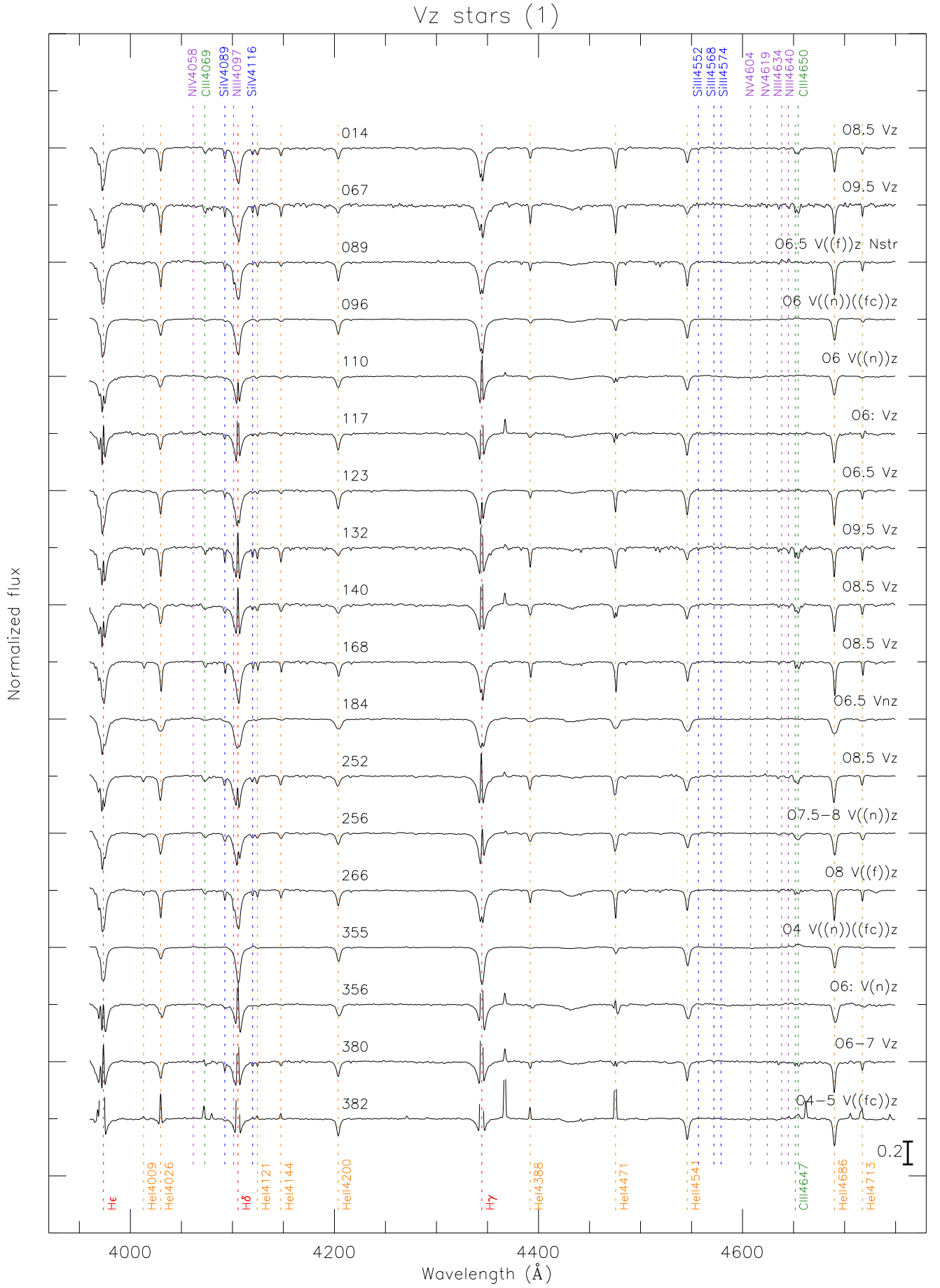


Fig. 13. VFTS Vz spectra.

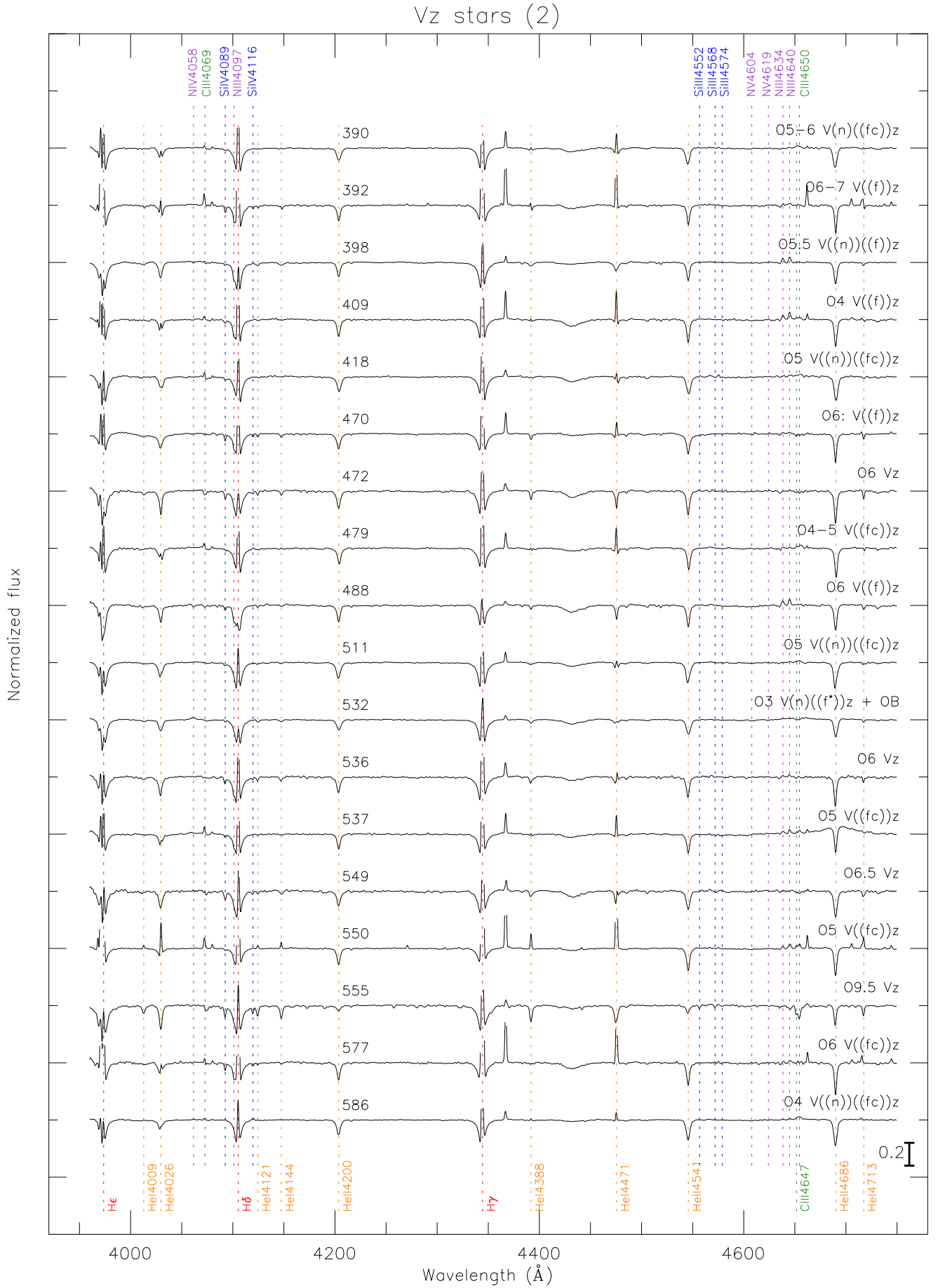


Fig. 14. Vz sample continued. VFTS 537 is contaminated by a nearby emission-line spectrum on the detector.

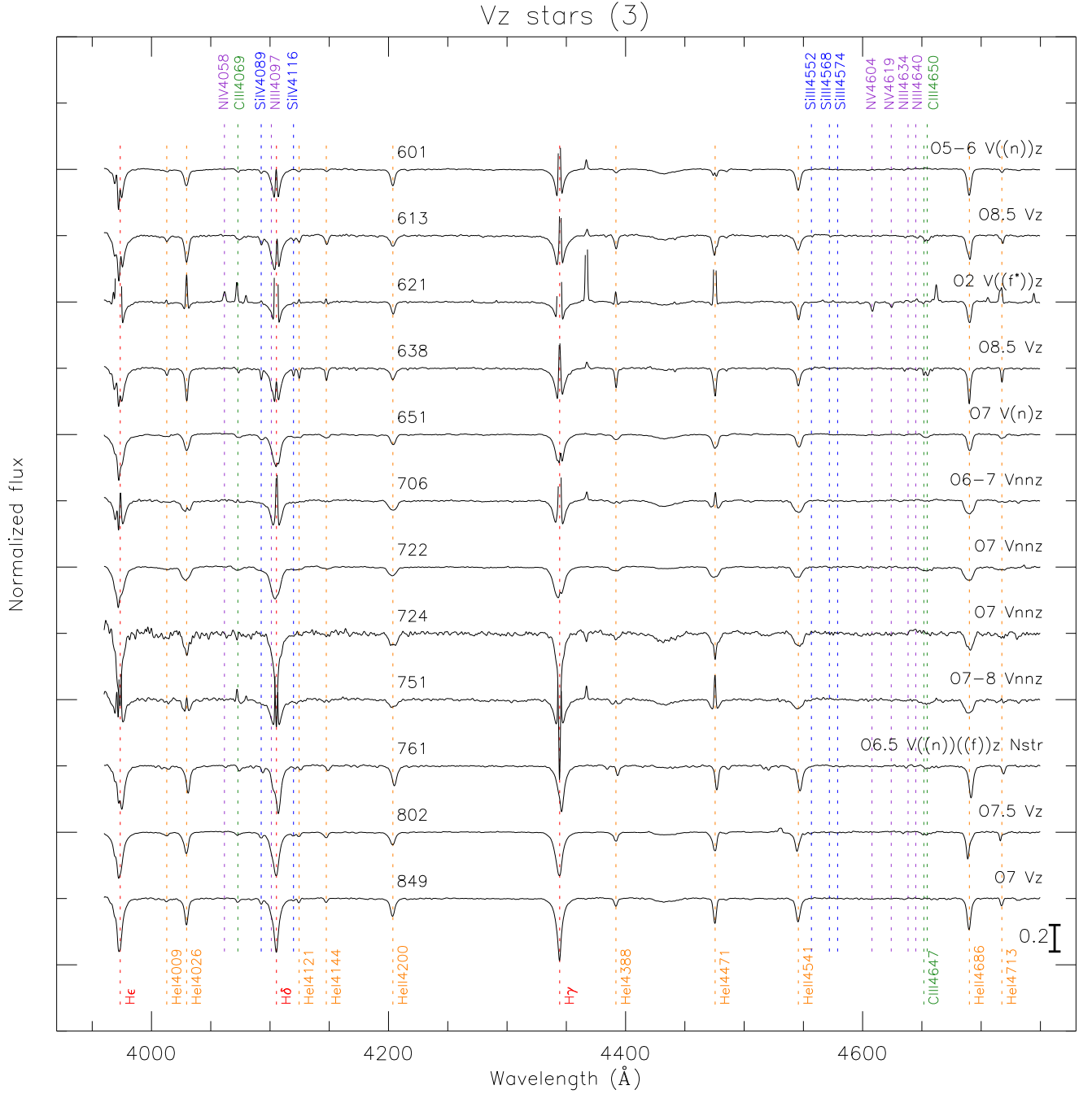


Fig. 15. Vz sample continued. VFTS 724 has oversubtracted nebular emission lines.

and there is nearly complete correspondence between no emission and Vz that may be consistent with extreme youth and weak winds (Rivero González et al. 2011).

3.6. Late-ON Spectra

A recent discussion of late-O, nitrogen-enhanced (ON) spectra was presented by Walborn et al. (2011); that paper specifically addressed rapid rotators, but it includes complete references to the general topic of N and C anomalies in O-type spectra, as well as possible evolutionary interpretations, that will not be replicated here. The morphology of these anomalies in luminous late-O spectra is quite distinctive. We have found only 3 such spectra

among the 213 VFTS O-type AAA data (VFTS 764, 807, 819), a result no doubt related to the evolved nature of such objects versus the youth of the majority of this sample. Note that all three are located near the southeastern edge of the observed field, far from the nebula. In fact, VFTS 764 = Sk −69° 252 belongs to an older, dispersed association far south of 30 Dor; it is the southernmost star marked in Fig. 2. Also note that despite its giant classification, VFTS 807 has a dwarf luminosity (Section 4 below). Nevertheless, these spectra are displayed in Figure 22, along with several morphologically normal spectra and one N weak (VFTS 045) of similar types in this sample. Although not associated with 30 Dor, these rare objects merit detailed physical analysis, since they are relevant to nuclear processing and

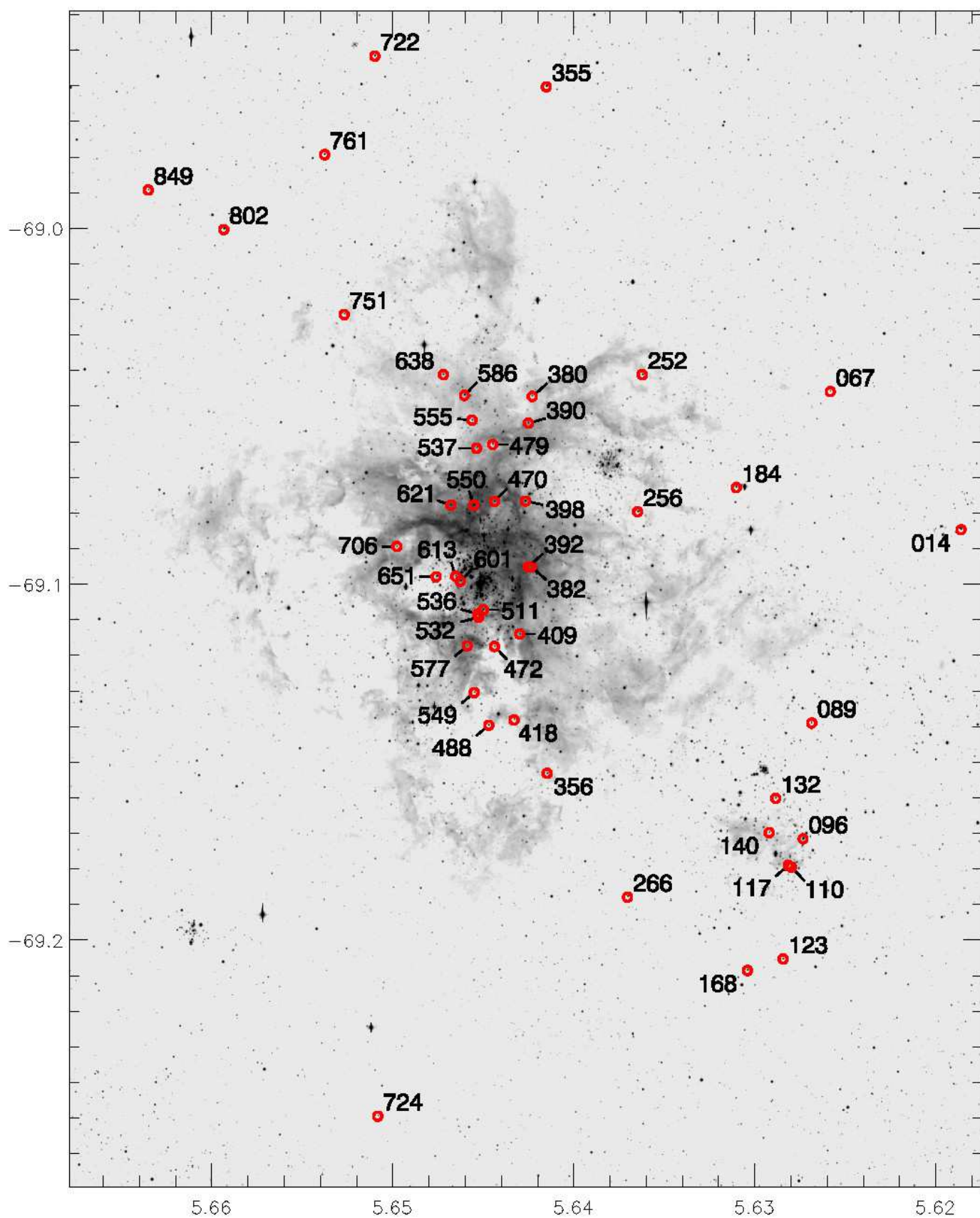


Fig. 16. Spatial distribution of the Vz stars.

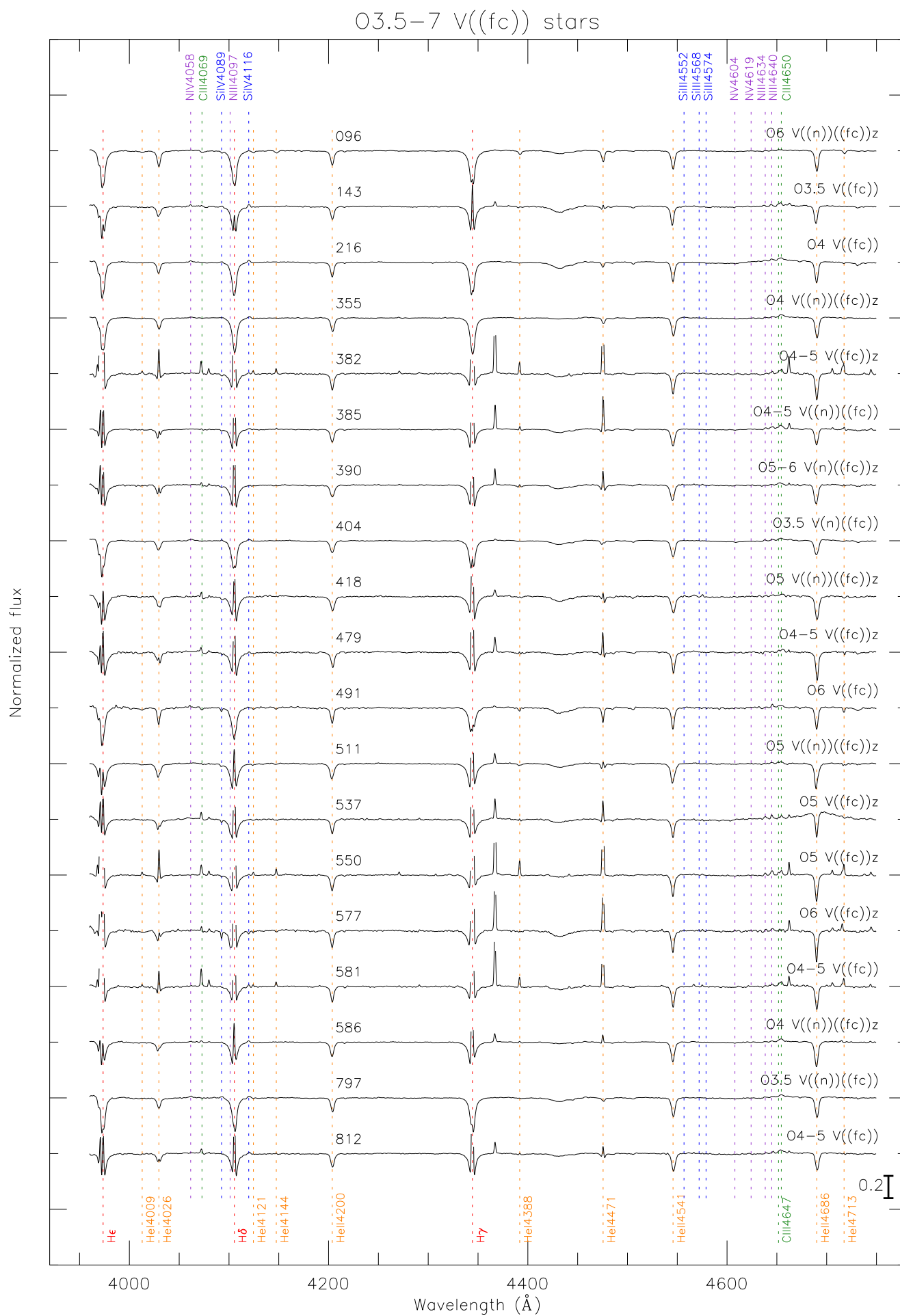


Fig. 17. VFTS V((fc)) spectra. VFTS 537 is contaminated by a nearby emission-line spectrum on the detector.

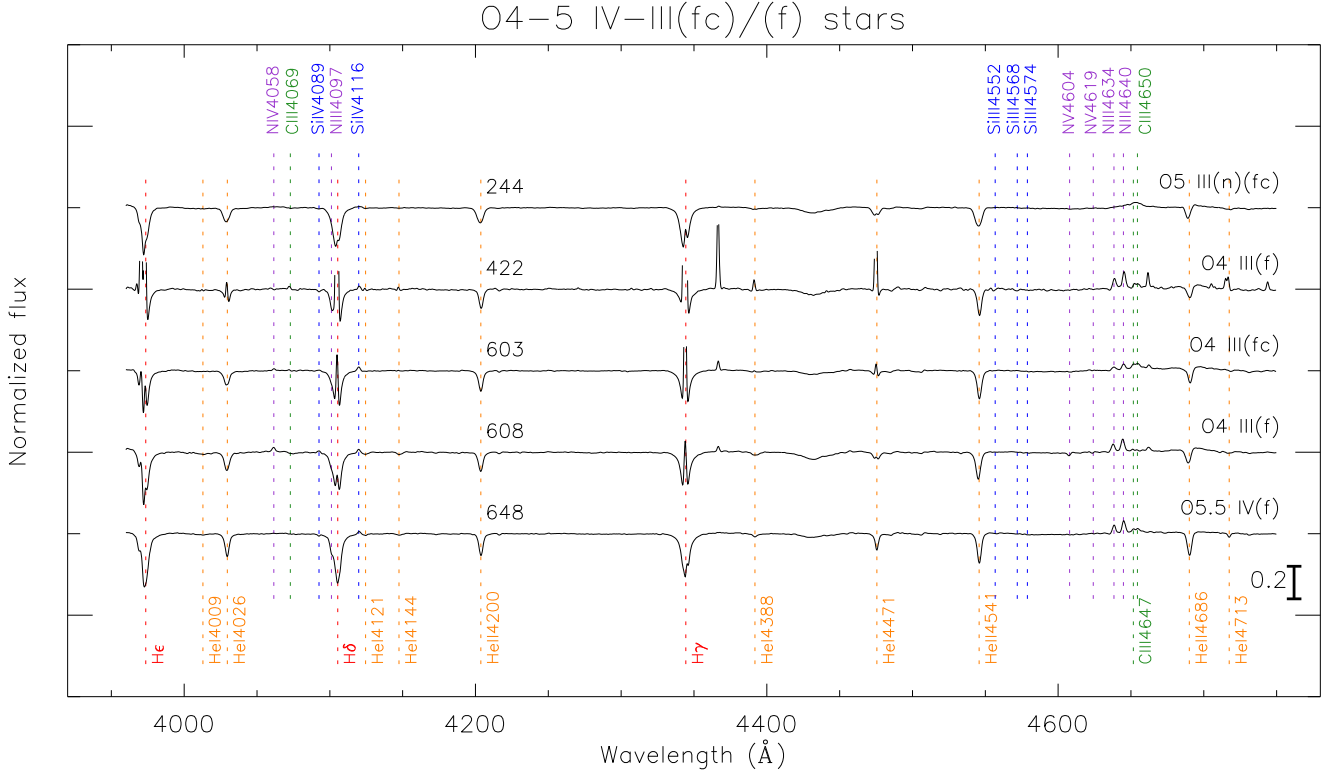


Fig. 18. VFTS III(fc) and III(f) spectra.

mixing or mass transfer in OB stars or binary systems of the corresponding mass and age ranges (Rivero González et al. 2012b).

3.7. Other Interesting Spectra

Several additional spectra of special interest at types O6–O9 are displayed in Figure 23. Most of them are not peculiar, but they are of relatively rare, luminous Of types so they are presented here for reference. Other spectra listed in Table 2 but not discussed and displayed in Section 3 will be posted on the VFTS public web page, as will those in Appendix A.

However, the spectrum of VFTS 318 is highly peculiar, even unique to date, so it is presented here even though it cannot be consistently classified and appears in the BBB list of Appendix A for that reason. The He II/He I line ratios would imply a type of O9.5 III, but the absence of any Si IV or other metal lines in the vicinity of H δ , together with the strong Balmer wings, produces the appearance of a B2 V spectrum there. Most remarkably, though, the spectrum also contains a narrow emission line of N IV λ 4058 and narrow absorption lines of N V λ 4604–4620, which if stellar would be characteristic of an O2 spectrum! The object is located well away from any clusters, indicating that it is not very young, unless it were a runaway. Moreover, it has a remarkably faint M_V of only -2.6 , corresponding to a normal B1–1.5 V star (Walborn 1972), so all of the O-type features must have an anomalous origin. The very high-ionization lines may originate in dilute material, perhaps compatible with their extremely narrow profiles; the possibility that they are excited by EUV or X-rays should also be considered. Alternatively, they would have to originate in a subluminal, very hot star. This object may be a result of advanced binary evolution; compatible with that possibility, radial-velocity variations indicate an SB.

4. Luminosities and HRDs

As indicated in Table 2, absolute visual magnitudes and physical parameters of most AAA stars have been derived; they are presented as Hertzsprung-Russell Diagrams (HRDs) in this Section.

The M_V and luminosity values were calculated with the Bayesian photometry package CHORIZOS (Maíz Apellániz 2004) and the following inputs: (a) the *BVJHK* photometry of Paper I; (b) effective temperatures derived from the spectral types of this paper and the calibration of Martins et al. (2005; to spectral type O3), shifted upward by 1000 K to account for the different metallicities of the Milky Way and the LMC (Rivero González et al. 2012a; Doran et al. 2013; whence the values for O2); and (c) a distance modulus of 18.5 as adopted by VFTS. The LMC stellar grid of Maíz Apellániz (2013a) was used, leaving three free parameters, which were determined for each star individually: (photometric) luminosity class, amount of extinction ($E(4405 - 5495)$), and type of extinction (R_{5495}). A wide range of the R values was found, the majority lying between 3 and 5 among the individual sightlines, with a few outliers reaching nearly 7. The extinction laws have been derived from the present spectral types, new WFC3 *UBVI* photometry, and Paper I *JHK* photometry (Maíz Apellániz 2013b; Maíz Apellániz et al. 2014). In a future paper of the VFTS series, we shall analyze the spatial distributions of $E(4405 - 5495)$ and R_{5495} , and their relationships with that of the Diffuse Interstellar Bands (van Loon et al. 2013).

4.1. Observational HRD

Figure 24 presents first the observational HRD (i.e., M_V vs. spectral type) for all 180 AAA stars with derived parameters. The M_V calibration of Walborn (1973), supplemented with values

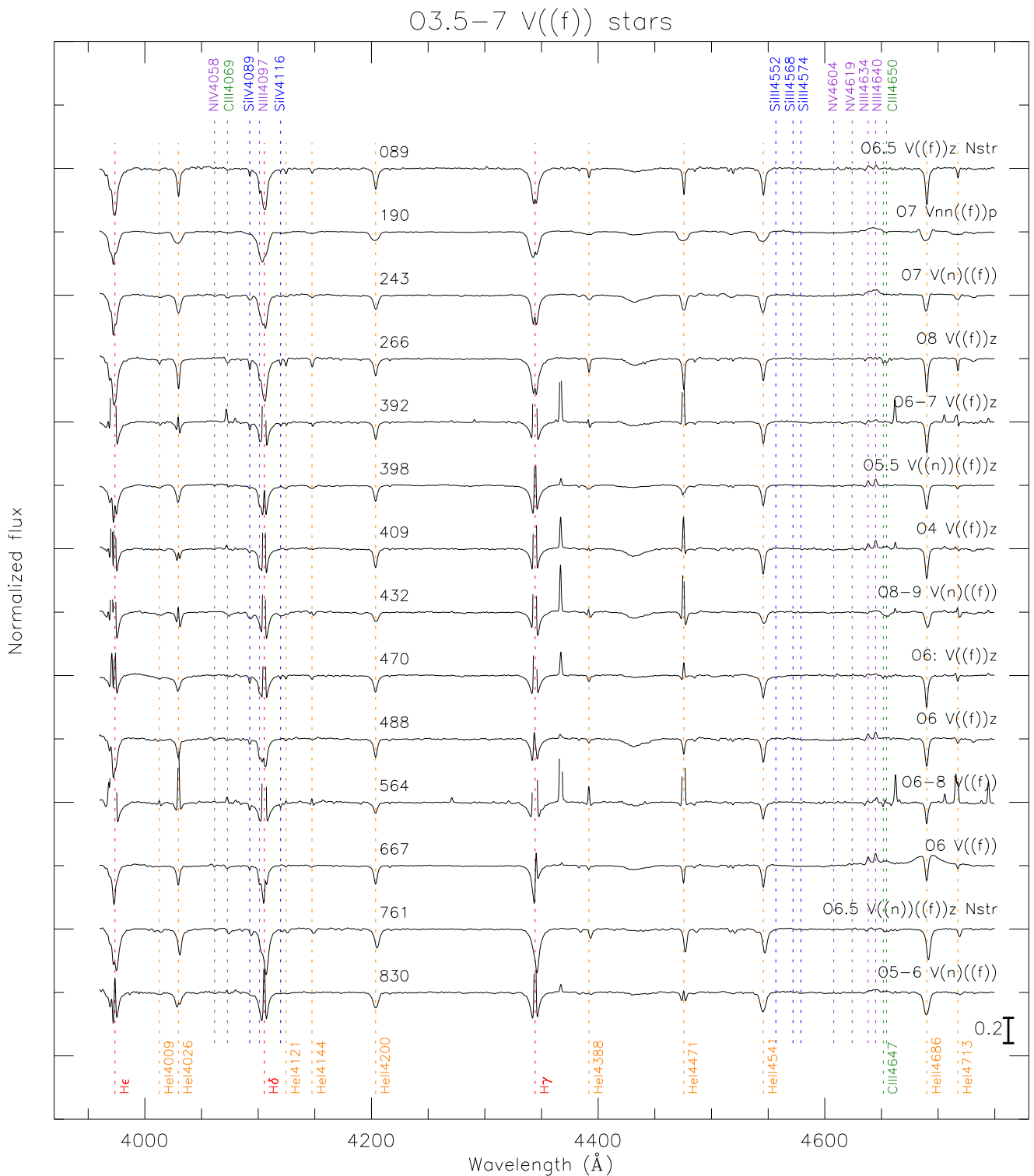


Fig. 19. VFTS V((f)) spectra. VFTS 667 is contaminated by a nearby emission-line spectrum on the detector.

for spectral types O2–O3 from Walborn et al. (2002a), is superimposed. There is reasonable agreement between the calibration and the individual magnitudes, with some scatter and exceptions. Individual magnitudes that are too bright are likely to be multiple systems; a case in point is VFTS 585 = Parker 1231 (spectral type O7 V(n) but $M_V = -6.19$), with equal components separated by only 0''.09 (Walborn et al. 2002b); it is in the AAA list and this HRD because it was missed in the initial survey of the WFC3

images, and to serve as a reminder of what remains below that limit. As is well known, the averaged luminosity class V calibration lies well above the ZAMS for O-type stars. In particular, most of the Vz stars fall below the class V line—as do a fair number of normal class V types, especially at the earliest and latest spectral types. This distribution is further discussed in the next Section.

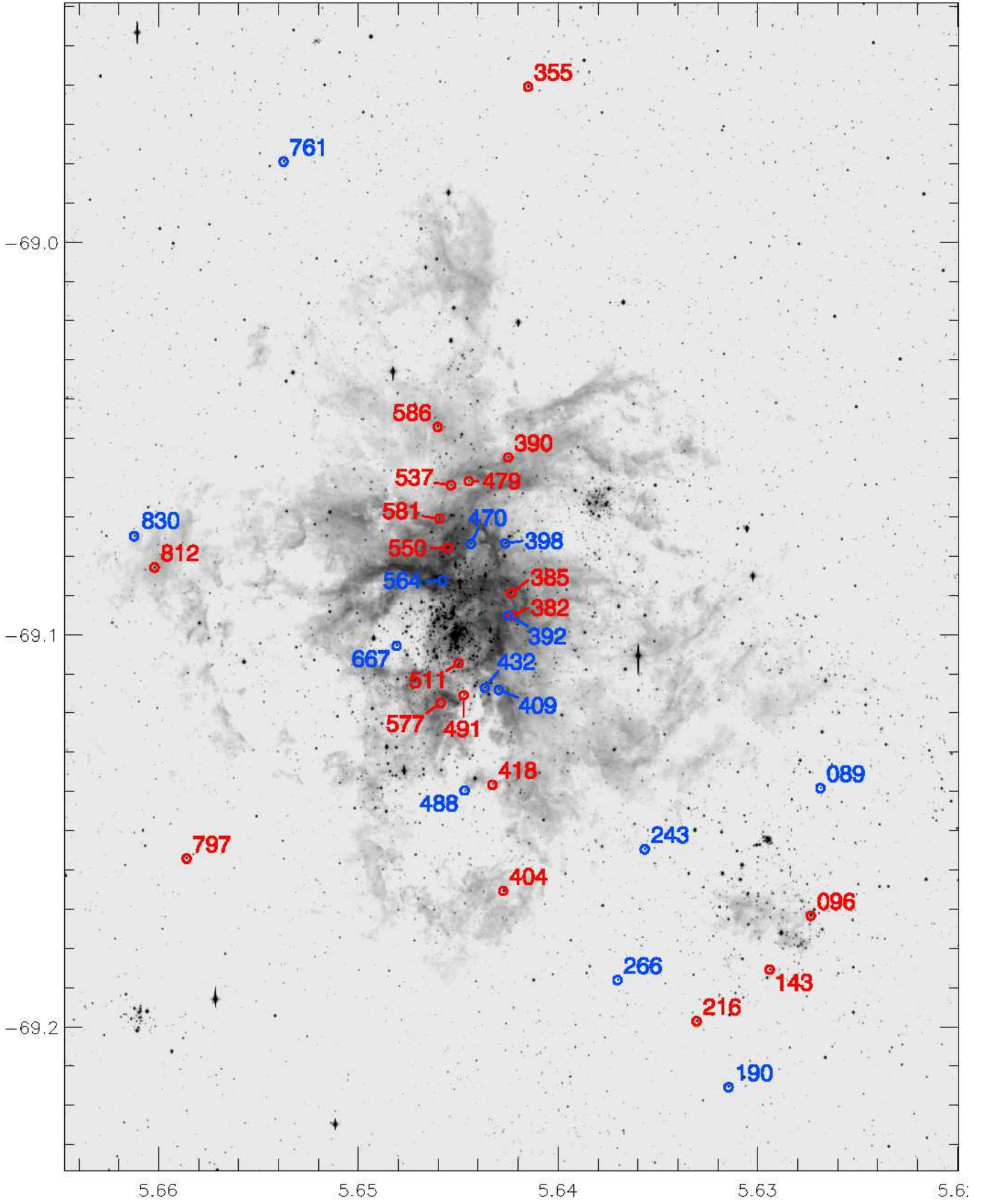


Fig. 20. Spatial distributions of V((fc)) (red) and V((f)) (blue) stars.

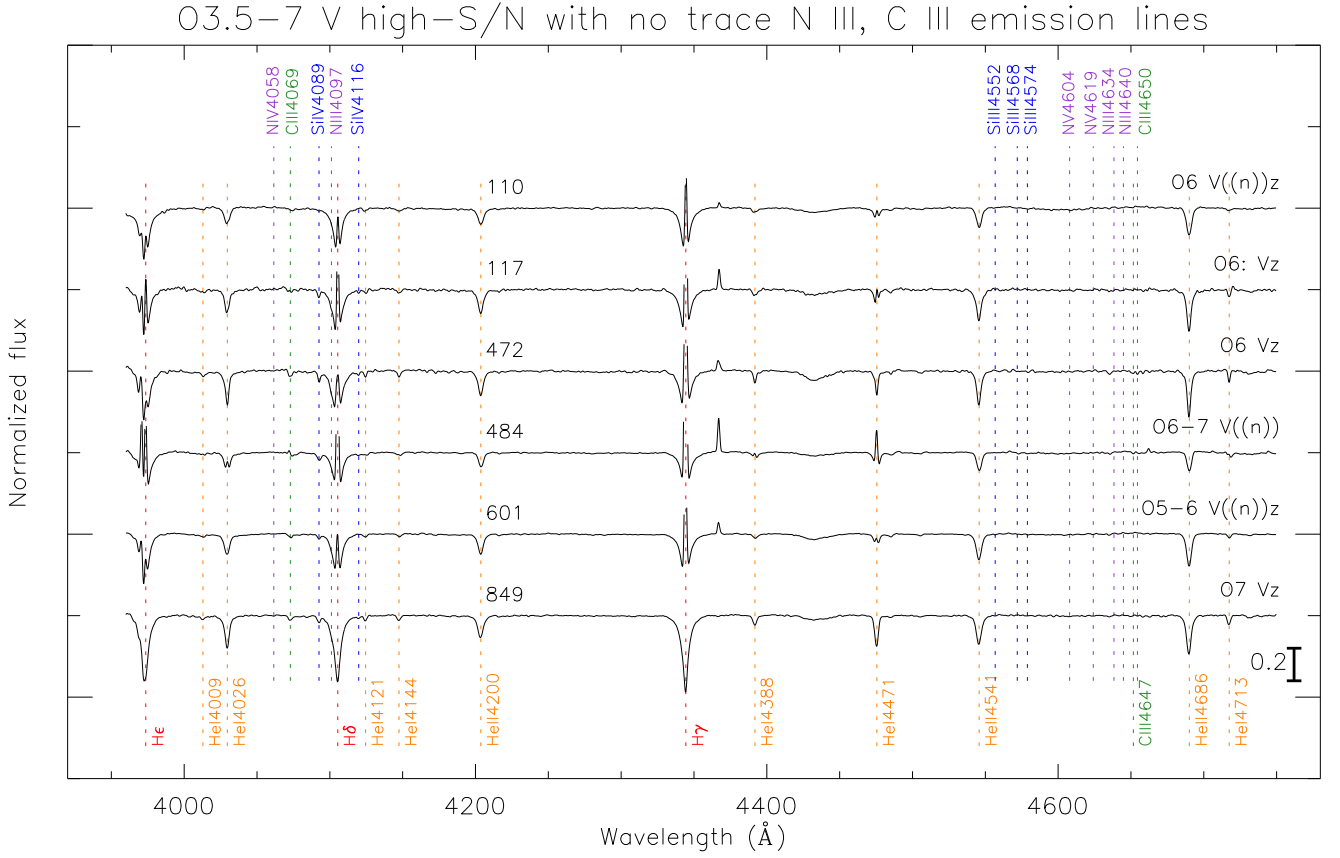


Fig. 21. VFTS class V spectra with high S/N but no trace of N III or C III emission lines.

Objects classified here as late-O giants but which fall among the dwarfs in the HRD are an important issue that is discussed in detail in the Appendix, in the context of a large number of BBB classifications with that property. An interrelated combination of classification and physical factors is likely involved. Some AAA objects in this category are seen in Fig. 24. The 5 worst cases, falling below the class V calibration line, are VFTS 210, 235, 574, 631, and 843; 574 and 843 are among the rapid rotators with giant classifications discussed in Section 3.2. There are also 7 cases just above the class V line, VFTS 012, 091, 399 (these 3 are also rapid rotators, completing that subset), 688, 753, 769, and 807. It is significant that VFTS 631 and 688 have remarks about weak Si IV lines in Table 2; VFTS 569 and 620 have related remarks, but are not in the HRD because no parameters could be derived for them. These 14 objects must be added to the related 39 BBB cases discussed in the Appendix.

Scatter between spectroscopic luminosity classifications of the OB stars and their derived absolute magnitudes is well known and has been often discussed, e.g., by Walborn (1973) who showed that the typical internal spread within associations is 0.5 mag. Scatter within 30 Dor was discussed by Walborn & Blades (1997). Systematic effects due to uncertainties in association distances and memberships were considered by Walborn (2002). In addition to the (physical) sources of random discrepancies noted in the previous paragraphs, differing reddening laws even within the same young region must be addressed, as we have done here. A more recently recognized issue is the effect of initial rotational velocity on evolutionary tracks; some striking possible examples in the SMC were found by Walborn et al. (2000) and analyzed by Hillier et al. (2003). Even more recently,

the fundamental effects of binary evolution are being elucidated (Sana et al. 2012; de Mink et al. 2013). Nevertheless, two-dimensional spectral classification remains an important method to chart the fundamental parameters of the majority of the stars, while discovering new categories and issues for further investigation.

4.2. Theoretical HRD

Figure 25 presents the theoretical (bolometric luminosity vs. effective temperature) HRD for the same stars as Fig. 24. Here the ZAMS, nonrotating evolutionary tracks, and isochrones for an LMC metallicity of $0.4 Z_{\odot}$ of Lejeune & Schaerer (2001) are also plotted. The isochrones are for ages of 1.0, 1.8, 3.2, 5.6, and 10.0 Myr. As previously known (e.g., Walborn & Blades 1997; Selman et al. 1999; Sabbi et al. 2012), a wide range of ages is present in the field of 30 Dor, even in the innermost region near R136. Nevertheless, a gap can be discerned between a sequence with ages 1–2 Myr and the remaining essentially continuous distribution older than about 3 Myr. All the stars are younger than 10 Myr, consistent with the O-type selection. (Trial HRDs were constructed only for stars within 80 pc of R136 in projection, but they appear essentially as sparser versions of the full-sample HRDs and so are not presented here.)

In view of the gap around that age in at least the upper HRD, stars with ages ≤ 2.5 Myr have been denoted by a “y” (for “young”) following the numeral in the HRD column of Table 2; this subgroup comprises all 32 analyzed stars with $T_{\text{eff}} \geq 41,900$ K plus 23 cooler ones. Their correlations with some of the special categories discussed above are considered

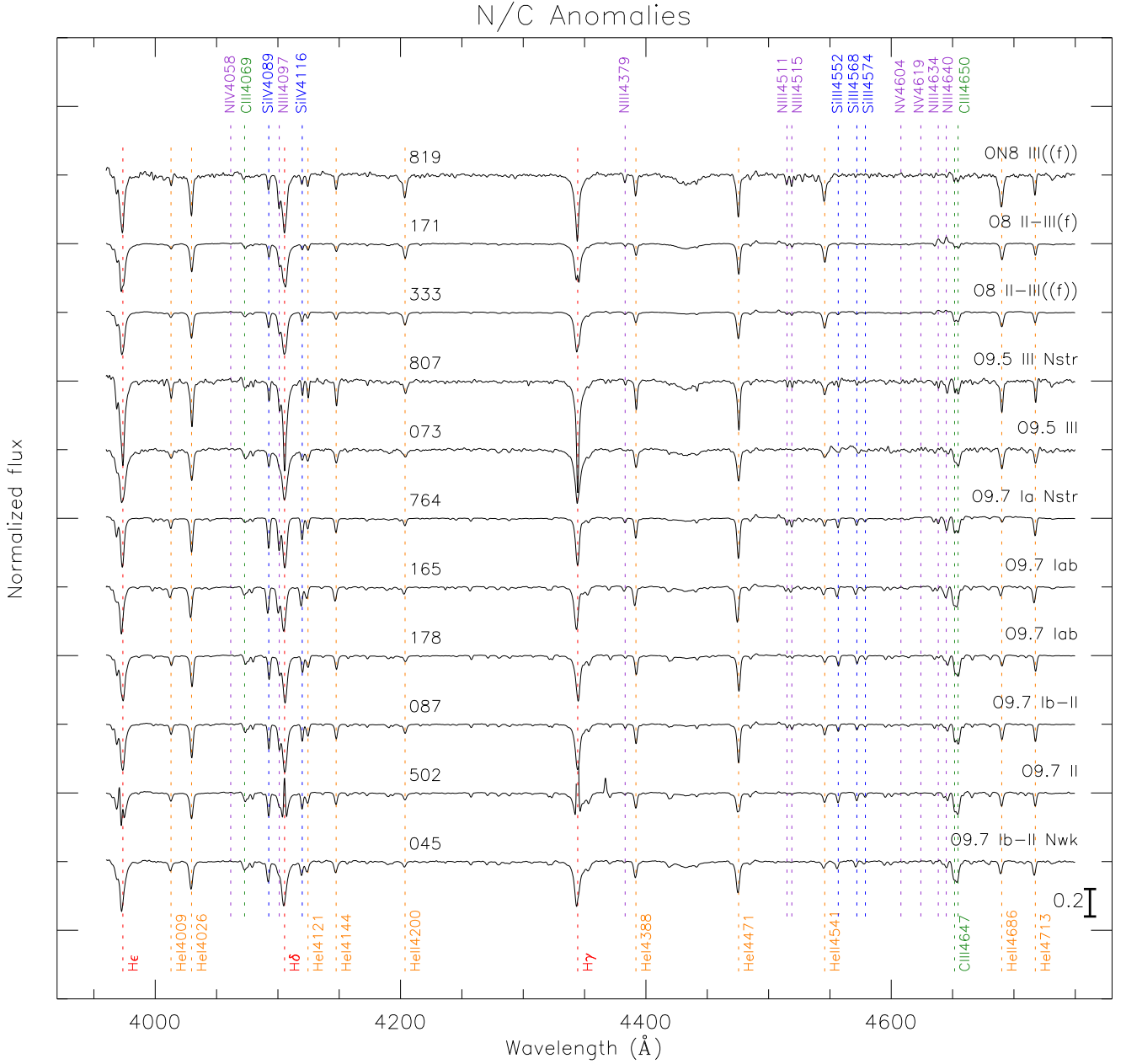


Fig. 22. VFTS spectra of luminous late-O stars with nitrogen and carbon anomalies, together with morphologically normal comparison spectra of similar types.

here. Most strikingly, 16/18 analyzed V((fc)) stars are in the young group. This result suggests a strong hypothesis that the characteristic may arise from a combination of the small LMC N/C abundance ratio and stellar youth, i.e., minimal internal mixing of processed material as yet. (It should be noted that the Galactic fc category discussed by Walborn et al. 2010b may have a different physical origin; some morphological distinctions between the Galactic and these 30 Dor spectra were pointed out in Section 3.5.) Interestingly, the two V((f))z stars with strong nitrogen lines mentioned in Section 3.4 are also in the young group; clearly their evolutionary path or status must be different from that of the V((fc)) objects.

Of the analyzed Vn/nn/nnn objects, 7/17 are in the young group, including the Vnnn VFTS 285, providing independent evidence of a runaway nature for those that have peripheral lo-

cations, as does the latter. Regarding the two Vnnz objects at the NS extremes of the field pointed out in Sections 3.2 and 3.4, VFTS 722 is in the young group while its opposite counterpart VFTS 724 just misses at about 3 Myr. In 2.5 Myr they would reach their current locations on the sky with respect to R136 at tangential speeds of 53 km sec^{-1} .

A further interesting feature of Fig. 25 is the distribution of the Vz stars, in comparison with that of their class V counterparts. First, it is seen that the majority of them are in fact among the youngest objects; 27/45 are in the young group just discussed, while only 10 of them lie significantly beyond the 3.2 Myr isochrone; at least some of the latter may be composite spectra simulating the Vz morphology, or otherwise multiple. However, a fair number of class V stars are also present in the younger domain—but predominantly at the highest and lowest

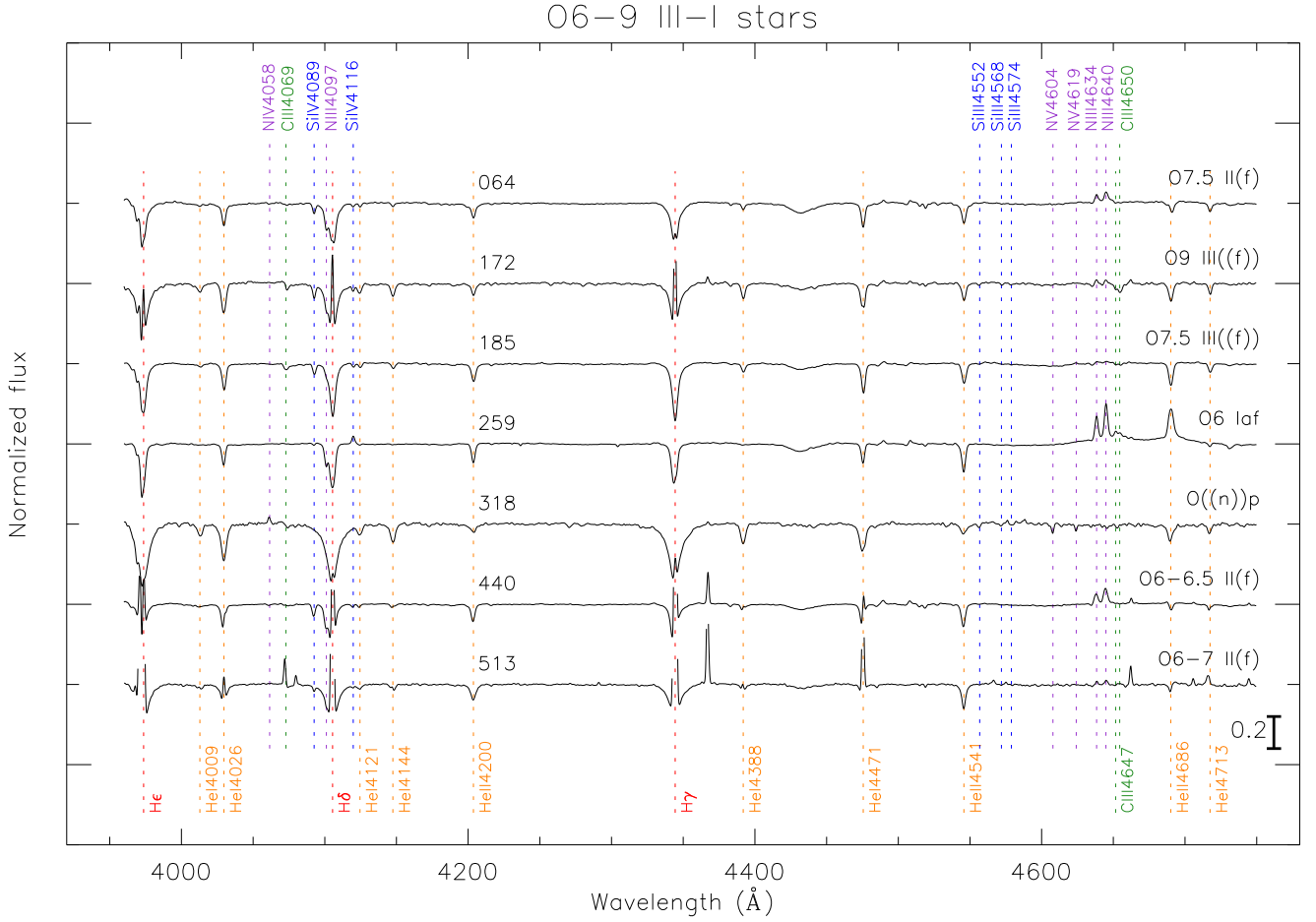


Fig. 23. Other interesting VFTS spectra.

temperatures (or earliest and latest O spectral types). The intermediate temperatures at the smaller ages are dominated by the Vz class; indeed, the *only* class V-IV (green square) point below the 1.0 Myr isochrone is VFTS 830, which is flagged as “z?” in Table 2. These results are consistent with the hypothesis of relatively small ages for that class, but with some complications that both expand knowledge and require explanation.

This peculiar relative T_{eff} /spectral-type distribution of the classes Vz and V spectra was first discovered and extensively discussed by Sabín-Sanjulián et al. (2014) in their astrophysical analysis of the same sample. In addition, they have shown that this T_{eff} distribution may be explained by He I and He II line-formation effects that tend to favor the Vz morphology at intermediate temperatures in 30 Dor; and that, to within the accuracy of the determinations, there is no separation in $\log g$ between the Vz and V stars. Finally, they offer the insight that the Vz phenomenon, which is related to reduced filling in of the He II $\lambda 4686$ absorption by wind emission, is expected to last longer and consequently be more frequent at the lower LMC metallicity with respect to the Galaxy, since the wind strengths depend on the latter. That may well be the reason for the surprisingly large number of Vz spectra in 30 Dor².

² The same effect may be an additional source of scatter in the present HRDs at higher luminosities, i.e., some objects may have luminosities underpredicted by their classifications because of weaker wind emission filling at $\lambda 4686$. Such a phenomenon would of course go in the opposite sense to the “subluminous giants” discussed elsewhere in this paper, in

Several factors in addition to the line-formation effects likely contribute to the relative dearth of Vz stars at the earliest and latest spectral types. At the former, winds are stronger and evolution more rapid, so that the Vz phase may well be shorter than at later types. It should also be noted that some early Vz spectra had to be dropped from the quantitative analysis, because of difficulties caused by the strong nebular contamination in their spectra. Factors relevant to the paucity of class Vz at late O spectral types may be the rapid decline of the Of effect at those types, and possibly longer embedded phases in the younger population that would push them below the VFTS limit because of higher extinction. Indeed, there is only one late-O star below the 1.8 Myr isochrone in Fig. 25, and it is a Vz (VFTS 638). On the other hand, the relatively larger number of class V at late types must also be an effect of the larger range of ages they represent; indeed, most of them lie *above* the 3.2 Myr isochrone.

It will be essential to analyze UV spectra of Vz and associated class V objects, to determine their mass-loss rates with higher accuracy than provided by differences in He II $\lambda 4686$ (or H α) absorption strengths alone. Attention is drawn to the extreme SMC OC6 Vz object NGC 346-113 for which both the optical and UV spectra are shown by Walborn et al. (2000). This star likely has the weakest wind known at that spectral type. Unfortunately, no UV spectra are yet available for the Vz sample in 30 Doradus, although *HST* is quite capable of obtaining them.

which the $\lambda 4686$ absorption is weaker than expected for their actual luminosities.

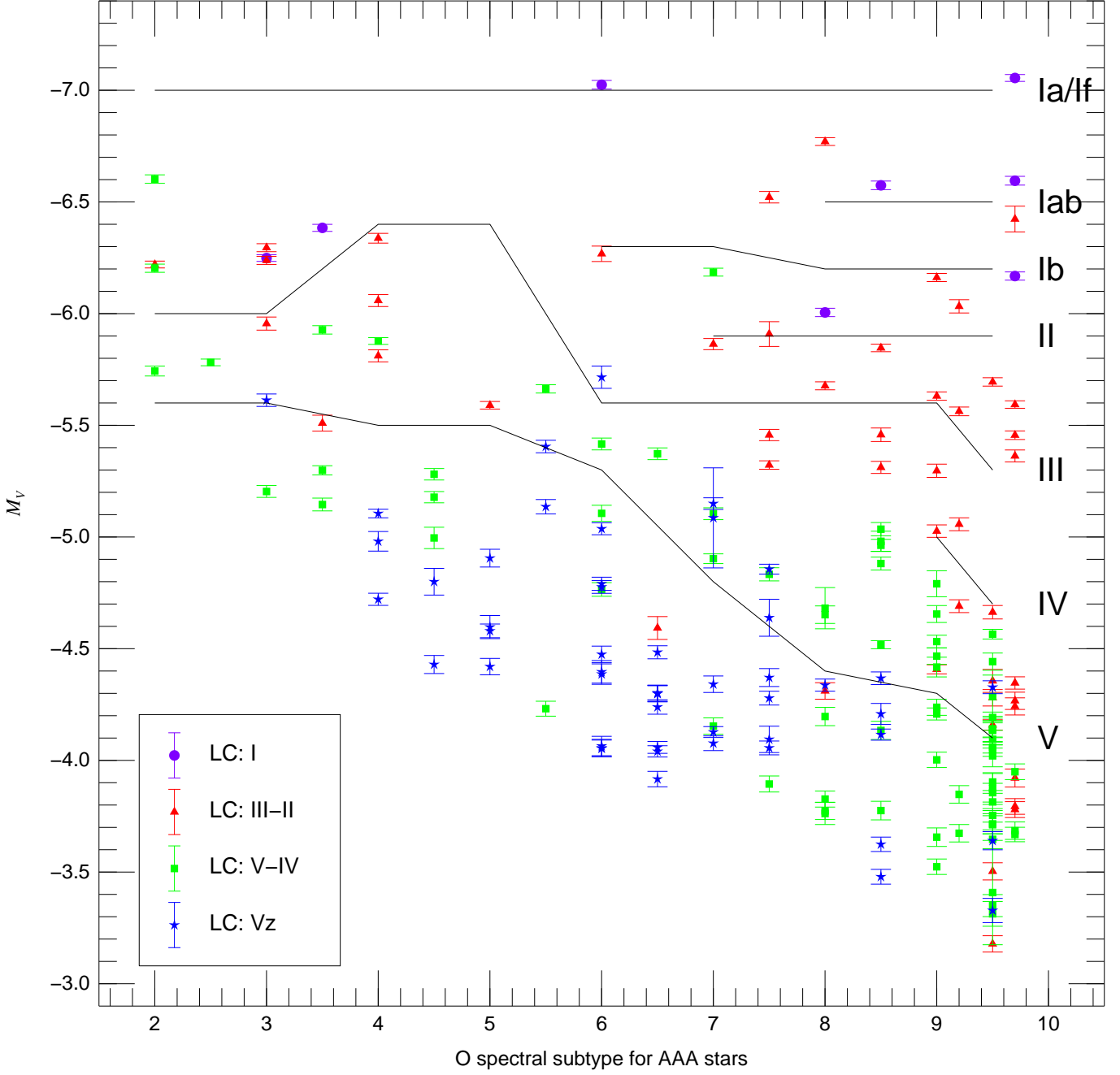


Fig. 24. Observational HRD, with the absolute magnitude calibration of Walborn (1973) superimposed.

5. X-Ray Sources

With observations from the *Chandra X-Ray Observatory*, Townsley et al. (2006) presented a study of point sources within the 30 Doradus Nebula. It is of interest to compare those results with the VFTS spectral classifications. The strongest X-ray point sources in 30 Dor are the composite WN6 + WC4 system R140N and the WN5h R136c, a bright member of the massive central core cluster. Other WR stars in the field are also among the stronger sources, due either to their massive winds or to binary-system mechanisms, as will be further discussed elsewhere. However, it is interesting that a very hard, likely nonthermal, and heavily extinguished source apparently associated with the

WN7h + OB system R135 could instead arise from the adjacent *Spitzer* source S3 discussed by Walborn et al. (2013).

As listed in the Tables 2 and A.1 comments, *Chandra* sources have been identified with 12 VFTS AAA O-type classifications and 6 BBB. The AAA sources include seven of types O2–O5 (VFTS 267, 468, 479, 506, 512, 601, 830), which may be reasonably hypothesized to have embedded stellar-wind shock origins, although five of them are also SB1 or composite. VFTS 333, 513, and 664 have bright giant luminosity classes, signifying He II $\lambda 4686$ significantly filled in by emission, which could however also be related to the X-rays. VFTS 564 is classified as a possible Oe star.

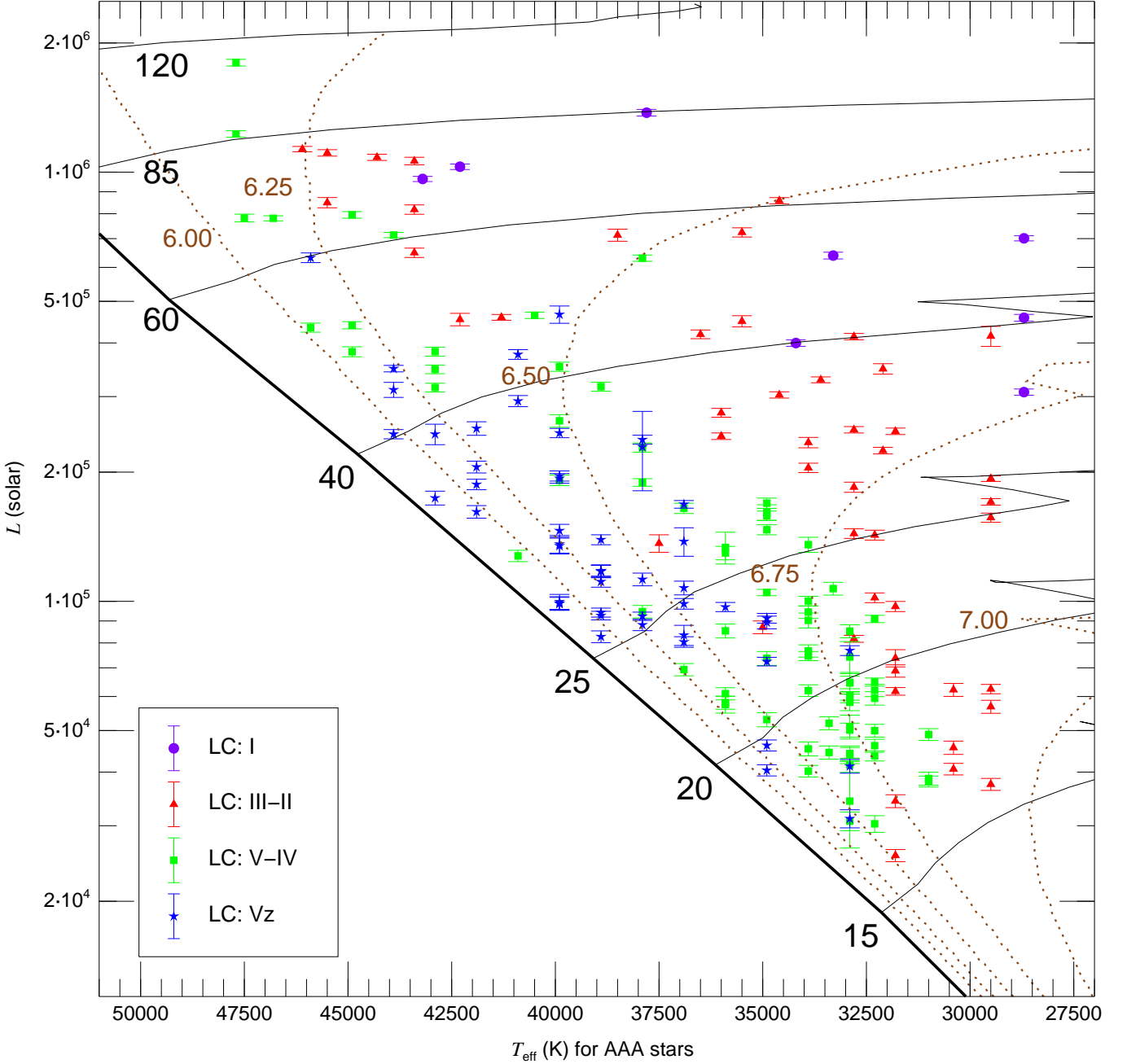


Fig. 25. Theoretical HRD of the full field, with evolutionary tracks specified by initial mass in solar units, and isochrones by log age.

However, the most intriguing X-ray source in the sample, VFTS 399, has the prosaic spectral type of O9 IIIIn, but with a dwarf M_V of only -4.4 , i.e., it is in the group of subluminescent “giants” discussed in Sections 3.2, 4.1, and A.2, with spectra displayed in Fig. 10. It is located in isolation a tenth of a degree south of R136. In one of three *Chandra* observations (Townsley 2012), it underwent a large flare lasting of order 10 ks, during which it became the third brightest source in 30 Dor, at about an order of magnitude above its quiescent level. The other observation had a flux intermediate between the two extremes. The source is very hard and likely nonthermal. Immediately upon learning of this behavior, we found very broad $H\alpha$ emission in

two VFTS observations and possible evidence for SB2 line profiles (Table 2). There appears to be a trend of order hundreds of days in VISTA K data, but no period could be discerned in OGLE I . Further investigation of these remarkable data is ongoing and will be reported elsewhere.

Four of the BBB sources are SB2 (VFTS 217, 445, 500, 527), while the other two (455, 579) are a large-amplitude SB1 and SB?, respectively. VFTS 527 = R139 is the massive O6.5 Iafc + O6 Iaf system discussed by Taylor et al. (2011). Colliding winds provide a likely hypothesis for the origin of the X-rays from these systems.

Table 3. Special Categories of VFTS O Stars with AAA-Rated Spectral Classifications

O2 (7)
016, 072, 169, 468, 506, 512, 621
O3 (11)
094, 143, 180, 267, 404, 518, 532, 566, 599, 755, 797
Vn/nn/nnn (18)
074, 138, 184, 190, 249, 285, 406, 592, 654, 660, 706, 722, 724, 746, 751, 755, 768, 770
V((n))/(n) high inclination? (10)
065, 072, 243, 250, 355, 356, 404, 761, 797, 830
III _n /nn (8)
012, 091, 399, 530, 531, 574, 615, 843
Onfp (7)
094(= ST1-28), 177, 190, 208(= ST1-93), 526, 626, 656
Vz (48)
014, 067, 089, 096, 110, 117, 123, 132, 140, 168, 184, 252, 256, 266, 355, 356, 380, 382, 390, 392, 398, 409, 418, 470, 472, 479, 488, 511, 532, 536, 537, 549, 550, 555, 577, 586, 601, 613, 621, 638, 651, 706, 722, 724, 751, 761, 802, 849
O3.5-7 V((fc)) (19)
096, 143, 216, 355, 382, 385, 390, 404, 418, 479, 491, 511, 537, 550, 577, 581, 586, 797, 812
O3.5-7 V((f)) (14)
089, 190, 243, 266, 392, 398, 409, 432, 470, 488, 564, 667, 761, 830
O3.5-7 V high-S/N with no trace of N III, C III emission lines (6)
110, 117, 472, 484, 601, 849
ON/N strong/N weak (7)
045, 089, 506, 761, 764, 807, 819
SB? from stellar/nebular shift (36)
021, 046, 067, 117, 123, 168, 169, 190, 216, 235, 251, 290, 306, 356, 418, 436, 491, 536, 549, 550, 586, 609, 620, 626, 639, 663, 664, 667, 679, 704, 710, 717, 722, 775, 777, 797

6. Summary and Outlook

This work provides basic spectroscopic descriptive information to complement and support a wide array of analyses undertaken by the various specialists of the diverse VFTS Team. Specifically, detailed spectral classifications have been presented for 352 O and B0 stars, many of which have been found to belong to several categories of special interest. These include the earliest (O2–O3) spectral types, of which nine new members have been found and for an equal number of which refined types are given. A salient result is the detection of a group of 18 very rapidly rotating O main-sequence stars, including the fastest known to date with $v \sin i \sim 600 \text{ km s}^{-1}$, for which radial-velocity and spatial distributions support a hypothesis of ejection from the 30 Dor clusters. Other noteworthy objects include new members of the also rapidly rotating but evolved Onfp class, and a surprisingly large number (48) of Vz objects, likely related to the lower metallicity and weaker winds in the LMC. They have been hypothesized to be in a very early evolutionary state, which is substantiated by their locations both on the sky and in

the HRDs, although further interesting aspects of their interpretation have emerged from parallel quantitative analysis as cited below. Further intricacies and diversity of O-type main-sequence spectral morphology have been uncovered, including 19 members of the O V((fc)) class with C III emission features equal to or stronger than the usual N III, as well as six with very high S/N but no trace of either emission species; this complexity will no doubt yield significant physical diagnostics when modeled and understood. Finally, several objects with morphological anomalies in their CNO spectra have been found, which are related to massive stellar evolution and mixing or transfer of processed material.

Basic information about VFTS has been provided by Evans et al. 2011 (Paper I), and further global analyses of these data from different perspectives have appeared or are in progress. Multiplicity among the O-type sample based on radial velocities has been investigated by Sana et al. (2013; Paper VIII) with the result that the spectroscopic binary fraction is at least 50%. The interstellar content of the spectra has been extracted by van Loon et al. (2013; Paper IX), including the detection of high-velocity absorption-line components in Na I; while the nebular emission-line data have been presented by Torres-Flores et al. (2013), revealing several new kinematic structures in the nebula. A census of the hot stars and their feedback, incorporating the present spectral classifications, has been compiled and discussed by Doran et al. (2013; Paper XI). The rotational velocities of the single O stars have been derived by Ramírez-Agudelo et al. (2013; Paper XII). The physical properties of the Vz class have been investigated by Sabin-Sanjulián et al. (2014; Paper XIII), providing important insights into its atmospheric and evolutionary significance. Detailed atmospheric and wind analyses of 62 VFTS O, Of/WN, and WN stars are presented by Bestenlehner et al. (2014; Paper XVII). Ultimately, exhaustive quantitative stellar spectral analysis of the full VFTS sample (complemented by *HST* spectroscopy in R136, PI P. Crowther; proper motions, PI D. Lennon; photometry, Sabbi et al. 2013), as well as studies of extinction (Maíz Apellániz et al. 2014; Paper XVI) and nebular lines, will support theoretical analyses of massive stellar evolution and the nebular environment, by means of which this unprecedented dataset for the unique 30 Doradus region will advance understanding of both massive stars and their starburst habitats.

Acknowledgements. We thank Leisa Townsley for providing the *Chandra* X-ray identifications together with parameter derivations prior to publication, and Selma de Mink for the *HST*/WFC3 image cutouts used to determine visual multiplicity among the target stars. We also thank our VFTS colleagues Paul Crowther, Selma de Mink, Artemio Herrero, Norbert Langer, Joachim Puls, and Jorick Vink as well as an anonymous referee for useful comments on the manuscript. STScI is operated by AURA, Inc. under NASA contract NAS 5-26555. SSD acknowledges funding by the Spanish Government Ministerio de Economía y Competitividad under grants AYA 2010-21697-C05-04, Consolider-Ingenio 2010 CSD2006-00070, and Severo Ochoa SEV-2011-0187, and by the Canary Islands Government under grant PID2010119. JMA acknowledges support from the Spanish Government Ministerio de Ciencia e Innovación through grants AYA 2010-17631 and AYA 2010-15081, and from the Junta de Andalucía through grant P08-TIC-4075.

References

- Allison, R.J., Goodwin, S.P., Parker, R.J. et al. 2010, *MNRAS*, 407, 1098
- Barbá, R.H., Gamen, R., Arias, J.I. et al. 2010, *RMxAA&ASC*, 38, 30
- Bestenlehner, J.M., Gräfener, G., Vink, J.S. et al. 2014, *A&A*, submitted
- Bestenlehner, J.M., Vink, J.S., Gräfener, G. et al. 2011, *A&A*, 530, L14
- Bosch, G., Terlevich, R., Melnick, J. et al. 1999, *A&AS*, 137, 21
- Breysacher, J., Azzopardi, M., & Testor, G. 1999, *A&AS*, 137, 117
- Brunet, J.P., Imbert, M., Martin, N. et al. 1975, *A&AS*, 21, 109
- Conti, P.S., & LEEP, E.M. 1974, *ApJ*, 193, 113

- Crowther, P.A., Schnurr, O., Hirschi, R. et al. 2010, MNRAS, 408, 731
- Crowther, P.A., & Walborn, N.R. 2011, MNRAS, 416, 1311
- Dale, J.E., & Davies, M.B. 2006, MNRAS, 366, 1424
- de Koter, A., Heap, S.R., & Hubeny, I. 1997, ApJ, 477, 792
- de Koter, A., Heap, S.R., & Hubeny, I. 1998, ApJ, 509, 879
- de Mink, S.E., Langer, N., Izzard, R.G. 2013, ApJ, 764, 166
- Doran, E.I., Crowther, P.A., de Koter, A. et al. 2013, A&A, 558, A134
- Dufton, P.L., Dunstall, P.R., Evans, C.J. et al. 2011, ApJ, 743, L22
- Evans, C.J., Lennon, D.J., Smartt, S.J. et al. 2006, A&A, 456, 623
- Evans, C.J., Taylor, W.D., Hénault-Brunet, V. et al. 2011, A&A, 530, A108
- Evans, C.J., Walborn, N.R., Crowther, P.A. et al. 2010, ApJ, 715, L74
- Feast, M.W., Thackeray, A.D., & Wesselink, A.J. 1960, MNRAS, 121, 337
- Fujii, M.S., & Portegies Zwart, S. 2011, Science, 334, 1380
- Hillier, D.J., Bouret, J.-C., Lanz, T. et al. 2012, MNRAS, 426, 1043
- Hillier, D.J., Lanz, T., Heap, S.R. et al. 2003, ApJ, 588, 1039
- Langer, N., Cantiello, M., Yoon, S.-C. et al. 2008, in IAU Symp 250, Massive Stars as Cosmic Engines, ed. F. Bresolin, P.A. Crowther, & J. Puls (Cambridge University Press), 167
- Lejeune, T., & Schaerer, D. 2001, A&A, 366, 538
- Maíz Apellániz, J. 2004, PASP, 116, 859
- Maíz Apellániz, J. 2013a, <http://adsabs.harvard.edu/abs/2013hsa7.conf..657M>
- Maíz Apellániz, J. 2013b, <http://adsabs.harvard.edu/abs/2013hsa7.conf..583M>
- Maíz Apellániz, J., Evans, C.J., Barbá, R.H. et al. 2014, A&A, in press
- Maíz Apellániz, J., Pellerin, A., Barbá, R.H. et al. 2012, ASPCS, 465, 484
- Maíz Apellániz, J., Sota, A., Walborn, N.R. et al. 2011, <http://adsabs.harvard.edu/abs/2011hsa6.conf..467M>
- Martins, F., & Hillier, D. J. 2012, A&A, 545, A95
- Martins, F., Schaerer, D., & Hillier, D. J. 2005, A&A, 436, 1049
- Massey, P., & Hunter, D.A. 1998, ApJ, 493, 180
- Melnick, J. 1985, A&A, 153, 235
- Parker, J.Wm. 1993, AJ, 106, 560
- Pasquini, L., Avila, G., Blecha, A. et al. 2002, Msngr, 110, 1
- Ramírez-Agudelo, O.H., Simón-Díaz, S., Sana, H. et al. 2013, A&A, 560, A29
- Rauw, G., Sana, H., Spano, M. et al. 2012, A&A, 542, A95
- Rivero González, J.G., Puls, J., Massey, P. et al. 2012a, A&A, 543, A95
- Rivero González, J.G., Puls, J., Najarro, F. 2011, A&A, 536, A58
- Rivero González, J.G., Puls, J., Najarro, F. et al. 2012b, A&A, 537, A79
- Roman-Lopes, A., Barbá, R.H., & Morrell, N.I. 2011, MNRAS, 416, 501
- Sabbi, E., Anderson, J., Lennon, D.J. et al. 2013, AJ, 146, 53
- Sabbi, E., Lennon, D.J., Gieles, M. et al. 2012, ApJ, 754, L37
- Sabín-Sanjulián, C., Simón-Díaz, S., Herrero, A. et al. 2014, A&A, in press
- Sana, H., de Koter, A., de Mink, S.E. et al. 2013, A&A, 550, A107
- Sana, H., de Mink, S.E., de Koter, A. et al. 2012, Science, 337, 444
- Sana, H., Dunstall, P.R., Hénault-Brunet, V. et al. 2012, ASPCS, 465, 284
- Sana, H., Rauw, G., & Gosset, E. 2001, A&A, 370, 121
- Sanduleak, N. 1970, Cerro Tololo Contribution, No. 89
- Schild, H., & Testor, G. 1992, A&AS, 92, 729
- Selman, F., Melnick, J., Bosch, G. et al. 1999, A&A, 347, 532
- Simón-Díaz, S., Castro, N., Garcia, M. et al. 2011, <http://adsabs.harvard.edu/abs/2011BSRSL..80..514S>
- Simón-Díaz, S., & Herrero, A. 2014, A&A, 562, A135
- Sota, A., Maíz Apellániz, J., Walborn, N.R. et al. 2011, ApJS, 193, 24
- Taylor, W.D., Evans, C.J., Sana, H. et al. 2011, A&A, 530, L10
- Testor, G., Llebaria, A., & Debray, B. 1988, ESO Messenger, No. 54, 43
- Torres-Flores, S., Barbá, R., Maíz-Apellániz, J. et al. 2013, A&A, 555, A60
- Townsley, L.K. 2012, STScI Workshop, 30 Doradus: The Starburst Next Door, <https://webcast.stsci.edu/webcast/detail.xhtml?talkid=3242&parent=1>
- Townsley, L.K., Broos, P.S., Feigelson, E.D. et al. 2006, AJ, 131, 2164
- van Loon, J.Th., Bailey, M., Tatton, B.L. et al. 2013, A&A, 550, A108
- Walborn, N.R. 1972, AJ, 77, 312
- Walborn, N.R. 1973, AJ, 78, 1067
- Walborn, N.R. 1976, ApJ, 205, 419
- Walborn, N.R. 2002, AJ, 124, 507
- Walborn, N.R. 2009, in STScI Symp. Ser., 20, Massive Stars from Pop III and GRBs to the Milky Way, ed. M. Livio & E. Villaver (Cambridge University Press), 167
- Walborn, N.R., Barbá, R.H., & Sewilo, M.M. 2013, AJ, 145, 98
- Walborn, N.R., & Blades, J.C. 1997, ApJS, 112, 457
- Walborn, N.R., Drissen, L., Parker, J.Wm. et al. 1999, AJ, 118, 1684
- Walborn, N.R., Howarth, I.D., Evans, C.J. et al. 2010a, AJ, 139, 1283
- Walborn, N.R., Howarth, I.D., Lennon, D.J. et al. 2002a, AJ, 123, 2754
- Walborn, N.R., Lennon, D.J., Heap, S.R. et al. 2000, PASP, 112, 1243
- Walborn, N.R., Maíz-Apellániz, J., & Barbá, R.H. 2002b, AJ, 124, 1601
- Walborn, N.R., Maíz-Apellániz, J., Sota, A. et al. 2011, AJ, 142, 150
- Walborn, N.R., Morrell, N.I., Howarth, I.D. 2004, ApJ, 608, 1028
- Walborn, N.R., Sana, H., Taylor, W.D. et al. 2012, ASPCS, 465, 490
- Walborn, N.R., Sota, A., Maíz Apellániz, J. et al. 2010b, ApJ, 711, L143

Table 2. AAA-Rated Spectral Classifications and Supporting Data for 213 VFTS O Stars

VFTS	SpT	V	$B - V$	M_V	T_{eff}	L/L_{\odot}	HRD	Mult	AltID	Comment
012	O9.5 III _n	15.83	0.15	-4.16	31800	6.17E4	1	runaway
014	O8.5 Vz	0	SBs
016	O2 III-If*	13.55	0.04	-6.22	46100	1.13E6	1y	runaway; Evans et al. 2010
021	O9.5 IV	15.57	0.09	-4.19	32300	6.49E4	1	SB?
045	O9.7 Ib-II Nwk	15.30	0.38	-5.46	29500	1.70E5	1	SBI	ST1-04	...
046	O9.7 II((n))	14.65	0.13	-5.36	29500	1.57E5	1	SB?	ST1-05	...
064	O7.5 II(f)	14.62	0.13	-6.52	35500	7.24E5	1	SB1s	ST1-12	...
065	O8 V(n)	15.99	0.06	-3.77	35900	5.81E4	1y
067	O9.5 Vz	16.83	0.16	-3.33	32900	3.12E4	1	SB?	...	He II wings
072	O2 V-III(n)((f*))	13.70	-0.14	-5.74	47500	7.82E5	1y	NC	BI253	runaway?
073	O9.5 III	16.14	0.38	-4.66	31800	9.73E4	1	SB11	ST1-19	...
074	O9 V _n	16.53	0.14	-3.66	33900	4.53E4	1	...	ST1-20	...
076	O9.2 III	15.24	0.19	-5.06	32300	1.43E5	1	...	ST1-21	...
086	O9 III((n))	14.47	0.12	-6.16	32800	4.14E5	1	SB11	ST1-24	...
087	O9.7 Ib-II	13.58	-0.14	-5.59	29500	1.93E5	1	SBvs
089	O6.5 V((f))z Nstr	16.08	0.20	-4.30	38900	1.17E5	1y	...	ST1-25	...
090	O9.5 V	15.78	0.19	0	SBI VM2?	ST1-26	...
091	O9.5 III _n	15.98	0.20	-4.36	31800	7.37E4	1	...	ST1-27	...
093	O9.2 III-IV	15.03	0.10	-4.69	32300	1.02E5	1	SBvs
094	O3.5 Inf*p + sec?	14.12	0.11	-6.38	42300	1.03E6	1y	SB2?	ST1-28	...
096	O6 V((n))((fc))z	13.91	0.00	-5.72	39900	4.66E5	1	SBvs VM2	ST1-29	...
098	O9 III(n)	15.07	0.15	-5.03	32800	1.44E5	1	SBI	ST1-30	...
103	O8.5 III((f))	16.20	0.47	0	VM2?	...	near O9
110	O6 V((n))z	15.69	0.07	-5.04	39900	2.47E5	1	VM2?	ST1-40	no emission lines
117	O6: Vz	16.64	0.18	-4.06	39900	9.89E4	1y	SB?	...	no emission lines
123	O6.5 Vz	15.78	0.10	-4.04	38900	9.26E4	1y	SB?	...	((fc))?
130	O8.5 V((n))	16.67	0.16	-4.52	34900	1.05E5	1
132	O9.5 Vz	16.09	0.07	-3.64	32900	4.13E4	1	...	ST1-51	He II broad
138	O9 V _n	15.63	-0.09	-3.52	33900	4.02E4	1	SB2?	...	runaway
140	O8.5 Vz	16.05	0.23	-4.37	34900	9.13E4	1	SBI	ST1-56	...
143	O3.5 V((fc))	15.36	0.19	-5.30	44900	4.40E5	1y	SB11	ST1-60	...
149	O9.5 V	16.44	0.16	-3.65	32900	4.15E4	2	...	ST1-61	...
154	O8.5 V	14.94	0.05	-5.04	34900	1.69E5	1	SBs	T88-7	Walborn et al. 1999 O7.5 V((f))
160	O9.5 III((n))	14.17	0.03	-5.69	31800	2.49E5	1	SB1s
165	O9.7 Iab	13.72	0.07	-6.17	28700	3.07E5	1	runaway
168	O8.5 Vz	15.46	0.08	-4.12	34900	7.24E4	1	SB?	...	He II broad
169	O2.5 V(n)((f*))	14.59	0.03	-5.78	46800	7.81E5	1y	SB?	ST1-71	C IV emission
171	O8 II-III(f)	14.06	-0.05	-5.68	34600	3.03E5	1	SBs	ST1-72	...
172	O9 III((f))	0	SBs	...	rare use of f at O9
177	O7n(f)p	14.63	0.24	-5.68	37900	3.91E5	0
178	O9.7 Iab	12.91	-0.05	-6.60	28700	4.58E5	1	SBvs	ST1-76	...
180	O3 If*	13.54	-0.08	-6.25	43200	9.64E5	1y	SBvs	ST1-78	Crowther & Walborn 2011
184	O6.5 Vnz	15.38	-0.09	-4.30	38900	1.18E5	2y	SBI
185	O7.5 III((f))	14.45	0.07	-5.32	36000	2.43E5	1	...	ST1-80	...
190	O7 Vnn((f))p	14.67	-0.04	-4.90	37900	1.89E5	1	SB?	...	runaway
191	O9.5 V	15.74	0.12	-4.06	32900	6.02E4	1	SB11	ST1-84	He II wings
197	O9 III	13.86	-0.06	-5.63	32800	2.51E5	1	SB11	ST1-87	...
208	O6(n)fp	14.65	0.33	-5.94	39900	5.77E5	0	SBs	ST1-93	...

continued on next page

Table 2. *continued*

VFTS	SpT	V	$B - V$	M_V	T_{eff}	L/L_{\odot}	HRD	Mult	AltID	Comment
210	O9.7 II-III((n))	15.60	0.00	-3.78	29500	3.75E4	2	...	ST1-94	...
216	O4 V((fc))	14.41	0.25	-5.88	43900	7.14E5	1y	SB?	ST1-97	...
223	O9.5 IV	14.77	-0.05	-4.56	32300	9.10E4	2	SBvs	ST1-101	...
235	O9.7 III	15.48	-0.06	-3.79	30400	4.07E4	2	SB?
243	O7 V(n)((f))	15.26	0.21	-5.10	37900	2.28E5	2	SB11
244	O5 III(n)(fc)	14.04	-0.10	-5.59	41300	4.59E5	2	SBvs
249	O8 Vn	15.52	-0.03	-3.83	35900	6.09E4	2y
250	O9.2 V((n))	15.74	0.02	-3.85	33400	5.20E4	2
251	O9.5 IV	15.62	-0.05	-3.81	32300	4.61E4	2	SB?	...	He II wings
252	O8.5 Vz	15.46	-0.13	-3.62	34900	4.62E4	2y
256	O7.5-8 V((n))z	15.02	-0.10	-4.28	36900	9.87E4	2	SB11
259	O6 Iaf	13.65	0.21	-7.02	37800	1.38E6	2	SB1s
266	O8 V((f))z	15.38	0.12	-4.34	35900	9.70E4	1
267	O3 III-I(n)f*	13.49	-0.05	-6.30	44300	1.08E6	2y	SB1vs	...	N V weak; X-ray source
277	O9 V	15.04	0.01	-4.53	33900	1.00E5	2	SB1
280	O9 V((n))	15.40	0.00	-4.24	33900	7.67E4	2
285	O7.5 Vnnn	15.63	-0.06	-3.89	36900	6.93E4	2y	runaway
290	O9.5 IV	15.67	0.04	-3.90	32300	5.00E4	2	SB?	...	He II wings
303	O9.5 IV	15.39	0.00	0	VM2	...	He II wings; Si IV weak
306	O8.5 II((f))	14.08	0.03	-5.85	33600	3.28E5	2	SB?	Mk80	runaway
332	O9.2 II-III	14.07	0.08	-5.56	32100	2.24E5	2	SB1s	Mk70 P32	...
333	O8 II-III((f))	12.49	-0.06	-6.77	34600	8.58E5	2	SBvs	R133 P42	X-ray source
355	O4 V((n))((fc))z	14.12	-0.19	-5.11	43900	3.48E5	1y	SB2 NC	...	runaway
356	O6: V(n)z	15.87	0.16	-4.47	39900	1.46E5	2y	SB?	P153	runaway
361	O8.5 V	15.82	0.02	-4.96	34900	1.58E5	2	...	P171	...
369	O9.7 V	16.66	0.15	-3.69	31000	3.86E4	2	...	P214	He II wings
380	O6-7 Vz	16.18	0.04	-3.92	38900	8.27E4	2y
382	O4-5 V((fc))z	15.88	0.14	-4.80	42900	2.45E5	2y
385	O4-5 V((n))((fc))	14.65	0.00	-5.18	42900	3.47E5	2y	SBs	P288	...
386	O9 IV(n)	14.75	0.20	0	SB11 VM2	Mk58(W) P294	Walborn et al. 2002b O7.5 V; inadvertently “Mk58(e)” in Paper I
390	O5-6 V(n)((fc))z	15.49	0.14	0	SB11	P316	...
392	O6-7 V((f))z	16.10	0.13	-4.48	38900	1.39E5	2
398	O5.5 V((n))((f))z	14.40	-0.03	-5.14	40900	2.93E5	2	SBvs	Mk59 P341	...
399	O9 IIIIn	15.83	0.08	-4.41	32800	8.18E4	1	SB2?	...	X-ray flare source; broad, variable H α emission
404	O3.5 V(n)((fc))	14.14	0.02	-5.93	44900	7.95E5	2y	SB11
406	O6 Vnn	14.30	0.01	-5.42	39900	3.52E5	2	...	Mk55 P370	contaminated; runaway
409	O4 V((f))z	15.75	0.59	-4.98	43900	3.11E5	2y	SB11	P404	...
410	O7-8 V	16.03	0.76	0	VM3	P409	Knot3; z? Walborn et al. 2002b, 2 components O8.5 V, O9 V
415	O9.5 V	15.48	-0.10	-3.41	32900	3.42E4	2	SB11	P466	...
418	O5 V((n))((fc))z	16.12	0.21	-4.42	41900	1.62E5	2y	SB?	P473	runaway
419	O9: V(n)	15.40	0.09	-4.79	33900	1.36E5	2	...	P485	...
422	O4 III(f)	15.14	0.24	-5.81	43400	6.49E5	2y	SB11
429	O7.5-8 V	14.69	-0.11	-4.83	36900	1.65E5	2	SB2	Mk57 P541	z?
432	O8-9 V(n)((f))	15.65	0.25	-4.98	34900	1.61E5	2	SB2?	P547	...
435	O7-8 V	16.86	0.53	-4.64	36900	1.38E5	2	...	P566	z?
436	O7-8 V	15.92	-0.05	-4.09	36900	8.34E4	2	SB?	...	z?
440	O6-6.5 II(f)	13.66	0.02	-6.27	38500	7.13E5	2	SB2?	Mk47 P607	...
441	O9.5 V	15.07	-0.07	-4.44	32900	8.52E4	2	SB2	P613	...
466	O9 III	15.60	0.37	-5.30	32800	1.84E5	2	...	P696	...

continued on next page

Table 2. *continued*

VFTS	SpT	V	$B - V$	M_V	T_{eff}	L/L_{\odot}	HRD	Mult	AltID	Comment
468	O2 V((f*)) + OB	14.59	0.04	0	VM4	Mk36 P706	C iv emission; X-ray source
470	O6: V((f))z	15.46	-0.08	-4.05	39900	9.87E4	2y	...	P716	...
472	O6 Vz	16.39	0.26	-4.06	39900	1.00E5	2y	...	P712	no emission lines
479	O4-5 V((fc))z	15.90	0.14	-4.43	42900	1.74E5	2y	SB11	P747	X-ray source
481	O8.5 III	14.16	-0.04	-5.46	33900	2.34E5	2	SB11	P9017	...
483	O9 V	16.38	0.12	0	SB?
484	O6-7 V((n))	15.07	0.14	-5.37	38900	3.16E5	2	no emission lines
488	O6 V((f))z	15.87	0.26	-4.79	39900	1.96E5	2	...	P791	...
491	O6 V((fc))	15.62	0.29	-5.11	39900	2.63E5	2	SB?	P803	...
493	O9 V	16.74	0.33	-4.42	33900	9.03E4	2
494	O8 V(n)	16.73	0.42	-4.20	35900	8.53E4	2	SB2?	P822	((f))?
498	O9.5 V	16.45	0.19	-4.29	32900	7.42E4	2
502	O9.7 II	13.76	0.07	-6.42	29500	4.15E5	2	SBvs	Mk27W P850	contaminated
503	O9 III	14.87	0.00	0	SB1vs	Mk27E	contaminated
505	O9.5 V-III	16.24	-0.02	0	VM2?
506	ON2 V((n))((f*))	13.31	0.02	-6.60	47700	1.80E6	2y	SB1s	Mk25 P871	X-ray source
508	O9.5 V	15.98	0.17	-4.13	32900	6.46E4	2	SB11	P872	...
510	O8.5 V	16.28	0.27	0	SB11
511	O5 V((n))((fc))z	15.28	0.12	-4.91	41900	2.53E5	2y	SB1s	P884	...
512	O2 V-III((f*))	14.28	0.20	-6.20	47700	1.23E6	2y	SB11	P885	X-ray source
513	O6-7 II(f)	16.20	0.06	-4.59	37500	1.36E5	2	near (fc); X-ray source
517	O9.5 V-III((n))	14.72	-0.08	0	...	Mk29 P909	...
518	O3.5 III(f*)	15.11	0.27	-5.51	42300	4.54E5	2y	SBs	P901	...
521	O9 V(n)	15.34	0.17	0	VM2	P905	...
526	O8.5 I((n))fp	14.92	0.54	-6.57	33300	6.39E5	2	SB11	P925	near O9
530	O9.5 III:nn	16.28	-0.02	0	SB1	P965	...
531	O9.5 III:nn	14.50	-0.11	0	SB11	Mk22W P983	runaway
532	O3 V(n)((f*))z + OB	14.76	0.20	-5.61	45900	6.32E5	2y	SB11 SB2?	P974	...
536	O6 Vz	16.21	0.23	-4.39	39900	1.35E5	2y	SB?
537	O5 V((fc))z	15.99	0.07	-4.58	41900	1.87E5	2y	...	P1022	contaminated
546	O8-9 III:((n))	15.36	0.04	0	...	P1052	...
549	O6.5 Vz	16.51	0.35	-4.30	38900	1.17E5	2y	SB?	P1063	...
550	O5 V((fc))z	15.25	0.09	-4.60	41900	2.06E5	2y	SB?	P1077	...
554	O9.7 V	16.61	0.04	0
555	O9.5 Vz	15.88	0.08	-4.33	32900	7.68E4	2	SB11	P1109	...
560	O9.5 V	16.59	0.05	-3.31	32900	3.07E4	2	...	P1139	He II wings
564	O6-8 V((f))	16.02	0.17	-5.09	37900	2.29E5	2	((fc))? z? Oe?; X-ray source
566	O3 III(f*)	14.05	0.06	-5.96	45500	8.49E5	2y	...	Mk23 P1163	...
569	O9.2 III:	16.09	0.07	0	...	P1170	p? discrepant He II λ 4686 vs. Si IV luminosity criteria
574	O9.5 III:n	15.89	-0.12	-3.18	31800	2.56E4	1	SB2? NC
577	O6 V((fc))z	16.64	0.40	-4.40	39900	1.36E5	2y	...	P1189	...
581	O4-5 V((fc))	16.07	0.18	-5.00	42900	3.15E5	2y	...	P1218	z?
582	O9.5 V((n))	16.83	0.16	0
585	O7 V(n)	13.65	0.12	-6.19	37900	6.30E5	2	SB11	P1231	Walborn et al. 2002b VM2: O6 V SB2?, O7 V
586	O4 V((n))((fc))z	15.04	-0.12	-4.72	43900	2.45E5	2y	SB?
592	O9.5 Vn	16.40	0.14	-3.72	32900	4.42E4	2
596	O7-8 V((n))	15.23	0.03	0	SB11 VM2	...	z?
597	O8-9 V(n)	15.56	0.03	-4.13	34900	7.36E4	2	...	P1288	...
599	O3 III(f*)	13.80	0.08	-6.24	45500	1.11E6	2y	SB1s	P1311	...

continued on next page

Table 2. *continued*

VFTS	SpT	V	$B - V$	M_V	T_{eff}	L/L_{\odot}	HRD	Mult	AltID	Comment
601	O5-6 V((n))z	14.69	0.09	-5.41	40900	3.76E5	2	...	Mk14N P1317	no emission lines; X-ray source
603	O4 III(fc)	13.99	0.04	-6.34	43400	1.06E6	2y	SB1I	Mk10 P1341	...
604	O8.5 V	14.94	0.04	-4.88	34900	1.47E5	2	SB2? VM2?	P1340	...
608	O4 III(f)	14.22	0.16	-6.06	43400	8.18E5	2y	SB1I	Mk14 P1350	...
609	O9-9.5 V-III	16.76	-0.01	0	SB?	P1354	...
611	O8 V(n)	16.16	0.13	-3.76	35900	5.75E4	2y
613	O8.5 Vz	15.78	0.16	-4.21	34900	8.93E4	2	SB1 VM2?	P1369	...
615	O9.5 IIIInn	15.89	0.02	0	VM3
619	O7-8 V(n)	15.98	0.12	-4.06	36900	8.04E4	2	SB1I	P1401	z?
620	O9.7 III(n)	16.61	0.03	0	SB?	P1416	Si iv weak
621	O2 V((f*))z	15.39	0.27	0	VM3	P1429	Knot2; ON? Walborn et al. 2002b O3-4 V
626	O5-6n(f)p	14.90	0.26	-5.62	40900	4.58E5	0	SB?	P1423	...
627	O9.7 V	15.38	-0.15	-3.67	31000	3.80E4	1	...	P9034	He II wings
630	O9.7 V-III	16.21	0.17	0	...	P1455	...
631	O9.7 III(n)	16.00	0.14	-3.92	30400	4.56E4	2	SB1	P1459	Si iv weak
635	O9.5 IV	15.52	0.07	-4.09	32300	5.94E4	2	SBvs	P1468	...
638	O8.5 Vz	15.63	-0.14	-3.48	34900	4.04E4	2y	He II broad
639	O9.7 V	15.41	-0.01	-3.95	31000	4.89E4	2	SB?
645	O9.5 V((n))	16.29	0.16	-3.86	32900	5.01E4	2	SB1	P1519	...
648	O5.5 IV(f)	14.16	0.08	-5.66	40500	4.64E5	2	SBvs	Mk8 P1531	C III emission but not (fc)
649	O9.5 V	16.07	0.05	-3.71	32900	4.40E4	2	SB2
651	O7 V(n)z	14.70	0.08	-5.15	37900	2.38E5	2	SB1I	Mk7 P1553	...
654	O9 Vnn	15.71	0.05	-4.21	33900	7.46E4	2	SB1	P1560	...
656	O7.5 III(n)((f))p	14.24	0.06	-5.46	36000	2.75E5	2	SB1I VM2?	Mk6 P1563	...
657	O7-8 II(f)	15.45	0.44	-5.91	35500	4.49E5	2	SB1I	P1573	...
660	O9.5 Vnn	15.92	0.03	0	...	P1586	...
663	O8.5 V	16.52	0.23	-3.78	34900	5.30E4	2	SB?	...	z? runaway
664	O7 II(f)	14.25	0.14	-5.86	36500	4.19E5	2	SB?	Mk4 P1607	X-ray source
667	O6 V((f))	15.03	0.07	-4.78	39900	1.93E5	2	SB?	P1614	z? contaminated
669	O8 Ib(f)	14.18	0.27	-6.01	34200	4.00E5	2	SB1s	P1619	...
677	O9.5 V	16.68	0.40	0	VM3	P1696	...
679	O9.5 V	16.73	0.25	-3.87	32900	5.10E4	2	SB?	P1698	He II wings
688	O9.7 III	15.60	0.11	-4.27	30400	6.22E4	2	SB1	P1756	Si iv a bit weak
702	O8 V(n)	16.31	0.33	-4.68	35900	1.34E5	2	SB1I	P1829	...
704	O9.2 V(n)	16.76	-0.07	0	SB?
706	O6-7 Vnnz	15.77	0.14	-4.24	38900	1.11E5	2y	...	P1838	...
710	O9.5 IV	16.14	-0.02	-3.35	32300	3.03E4	2	SB?	P1849	He II wings
716	O9.5 IV	15.91	0.06	-4.14	32300	6.20E4	2	SBs	P1890	...
717	O9 IV	15.69	0.19	-4.66	33300	1.07E5	2	SB? VM?	P1892	...
722	O7 Vnnz	15.04	-0.13	-4.08	37900	8.81E4	1y	SB? NC	...	runaway
724	O7 Vnnz	16.80	0.43	-4.34	37900	1.12E5	1	NC	...	nebular lines oversubtracted; runaway?
736	O9.5 V	15.85	0.05	-4.14	32900	6.47E4	2	SB1I VM2?	P1998	He II wings
737	O9 V	15.70	0.13	-4.47	33900	9.44E4	2	...	P2000	z? He II broad
743	O9.5 V((n))	15.04	-0.17	-4.05	32900	5.98E4	1	SB1I NC
746	O6 Vnn	15.38	0.12	-4.77	39900	1.91E5	2
750	O9.5 IV	15.43	-0.11	-3.75	32300	4.36E4	1	SB1I NC
751	O7-8 Vnnz	16.32	0.15	-4.37	36900	1.07E5	2	NC
753	O9.7 II-III	16.46	0.42	-4.35	29500	6.25E4	1	NC	...	He II wings; sharp lines; H γ p
755	O3 Vn((f*))	15.04	0.14	-5.20	45900	4.34E5	2y	...	P2041	C IV emission; runaway

continued on next page

Table 2. *continued*

VFTS	SpT	V	$B - V$	M_V	T_{eff}	L/L_{\odot}	HRD	Mult	AltID	Comment
761	O6.5 V((n))((f))z Nstr	15.35	-0.13	-4.06	38900	9.42E4	1y	NC	...	runaway
764	O9.7 Ia Nstr	12.26	0.09	-7.06	28700	7.01E5	1	SB1s NC	Sk-69° 252	...
768	O8 Vn	16.10	0.20	-4.65	35900	1.30E5	1	SB2? NC
769	O9.7 II-III	15.83	0.08	-4.24	29500	5.68E4	2	SB1	P2099	...
770	O7 Vnn	15.79	0.08	-4.15	37900	9.46E4	2y
775	O9.2 V	16.85	0.29	-3.67	33400	4.44E4	1	SB? NC	...	He II wings
777	O9.2 II	15.30	0.38	-6.03	32100	3.48E5	1	SB? NC
778	O9.5 V	16.64	0.14	-4.02	32900	5.82E4	2
782	O8.5 III	15.47	0.36	-5.31	33900	2.05E5	1	NC
797	O3.5 V((n))((fc))	14.68	0.05	-5.15	44900	3.82E5	2y	SB?	...	runaway
802	O7.5 Vz	14.14	-0.19	-4.86	36900	1.68E5	1	SB2 NC	BI258	...
807	O9.5 III Nstr	16.37	0.56	-4.28	31800	6.88E4	1
812	O4-5 V((fc))	14.81	0.05	-5.28	42900	3.82E5	2y	SB11	P2246	...
819	ON8 III((f))	16.79	0.40	-4.31	35000	8.70E4	1	NC
830	O5-6 V(n)((f))	15.39	-0.03	-4.23	40900	1.28E5	2y	SB1	P2270	((fc))? z? X-ray source
843	O9.5 IIIIn	15.88	-0.05	-3.50	31800	3.42E4	1	NC
849	O7 Vz	15.14	-0.08	-4.13	37900	9.23E4	1y	NC	...	no emission lines
892	O9 V	15.69	0.05	-4.00	33900	6.19E4	1	NC	...	He II broad

Notes. Entry code explanations: HRD column: 0, not included in the HRDs (Section 4) because of no or uncertain luminosity class, visual multiplicity, no photometry or poor SED fit (33 stars); 1,2, included in the HRDs (180 stars); 2, within 80 pc projected of R136 (117 stars); y, age ≤ 2.5 Myr per HRD (55 stars). Multiplicity column: SB, spectroscopic binary; 1, single lined; 2, double lined; l, large amplitude ($>20 \text{ km s}^{-1}$); s, small amplitude ($10\text{--}20 \text{ km s}^{-1}$); vs, very small amplitude ($<10 \text{ km s}^{-1}$); SB?, stellar absorption displaced from nebular emission lines but no radial-velocity variation measured; VMn, visual multiple of n components within $1''.2$ Medusa fiber, as determined in *HST*/WFC3 image; NC, no WFC3 coverage. 140/213 stars have SB, VM, or both entries; moreover, multiples with separations between about 5000 AU and 1 AU (or less than the latter with unfavorable inclinations) would not, in general, be detected by either technique, except that some SB? may be within that gap. On the other hand, some SB? may instead have high velocities relative to the gas. Alternate ID column sources: ST1, Schild & Testor 1992; BI, Brunet et al. 1975; T88, Testor et al. 1988; Mk, Melnick 1985; P, Parker 1993; R, Feast et al. 1960; Sk, Sanduleak 1970.

Appendix A: BBB Classifications

The Appendix addresses 139 objects in the VFTS O–B0 sample with lower-rated (“BBB”) spectral classifications, which are largely excluded from the discussion in the main text as well as entirely from the HRDs. They are listed in Table A.1. The reasons for the lower ratings are discussed next. These spectra are not displayed in this paper (except for VFTS 318 in Fig. 23) but will be at the VFTS website.

A.1. Reasons for Lower-Rated Classifications

There are several distinct reasons for the BBB classifications. The most obvious are relatively low S/N of the data and/or severe nebular contamination at the He I lines, which render the classifications uncertain and frequently preclude luminosity classes. Of course, these cases are generally among the fainter stars in the sample. Table A.1 also contains 10 B0 spectra to define the O–B boundary; some of them are of fine quality.

A second BBB category comprises the majority of the prominent SB2. While the data quality for these is often excellent, they cannot be included in the HRDs without full orbital analyses, which in general require further observations that are in progress. (A few SB2 that were recognized later are included in the AAA list and HRDs, as are of course any that remain undetected; in general, they may be expected to have relatively fainter and less contaminating secondaries.) As already noted, the SB2 have been classified by JMA with MGB using the best data near quadratures; while some of these classifications are necessarily uncertain, others are fine.

The most vexing BBB category is discussed separately in more detail in the following section.

A.2. He II $\lambda 4686$ vs. Si IV Luminosity Criterion Discrepancies at Late-O Types

Thirty-nine of the 139 BBB spectra fall into this category, as do 14 AAA types discussed in Section 4.1; other late-O BBB also have weak Si IV but luminosity classes could not be derived. While the classical MK procedure in general relied upon subjective averages over (sometimes mildly conflicting) multiple criteria, the tendency in this work (as well as in GOSSS; Sota et al. 2011) is to define a primary criterion for each subcategory, in the interests of clarity and reproducibility. In the case of luminosity classification at late-O types, the He II $\lambda 4686$ /He I $\lambda 4713$ luminosity criterion, which decreases with increasing luminosity due to emission filling in the He II absorption line, has been preferred over the Si IV/He I ratios because of the susceptibility of the latter to metallicity effects. Rather severe discrepancies between the two criteria are encountered in many of the 30 Dor spectra at these types (as well as less frequently in the Galaxy).

Thus, this approach has unfortunately not been entirely successful in the current sample. While the different criteria agree for many late-O types in the AAA list, for a few as well as for numerous BBB they do not. A contributing factor may well be that the late-O horizontal classification criterion Si III $\lambda 4552$ /He II $\lambda 4541$, the unit value of which defines type O9.7, is also sensitive to metallicity. This dependence, in combination with the rapid decline of the luminosity-dependent He II $\lambda 4686$ emission filling with advancing type in this range, such that He II $\lambda 4686$ /He I $\lambda 4713$ has similar values near unity at O9.7 II and B0 IV, entails substantial interrelated uncertainties in both dimensions. However, additional sources of He II $\lambda 4686$ emission unrelated to luminosity in this young LMC sample cannot be excluded a priori. It also appears that blended multiples may be another source of this problem; several cases in which spectral classifications from *HST* data yielded lower luminosity classes are noted in the Table A.1 Comments (VFTS 141, 150, 153, 389). It is likely that quantitative spectral analysis and in some cases observations with higher spatial resolution will be required to fully elucidate these issues.

To quantify this problem further, the average absolute visual magnitudes of the 12 AAA and 24 BBB stars in this category with parameters are compared to the predictions from their luminosity classes here. The observed M_V ’s available for the BBB objects are listed in the Comments field of Table A.1; as for the discrepant AAA, the observed values are fainter than the calibration predictions (Walborn 1973) in all but one case (VFTS 389, ironically one of those with a fainter *HST* luminosity class). For 25 stars classified O9.5–O9.7 III, the average observed value is -3.86 ± 0.10 (m.e.), compared with a calibration value of -5.3 . For six O9.5–O9.7 II–III and two O9 III, the observed value is -4.34 ± 0.12 , whereas the calibration values are -5.6 . There is one O9.5 II with an observed -4.6 but calibration -5.9 ; and one O9.5 IV with values of -3.8 vs. -4.7 , respectively, but another (VFTS 389) with a brighter observed value of -5.1 . The observed values do increase toward brighter luminosity classes, but except for the two class IV stars, the observed minus predicted are remarkably consistent at 1.3–1.4 mag, as also with the O9.5–O9.7 V calibration value of -4.1 and what would have been predicted from the small Si IV/He I ratios. On the other hand, for three B0 V stars (VFTS 347, 496, 540) the observed values are more consistent with the calibration, average -3.5 vs. -3.6 (Walborn 1972), respectively, so that some of the apparent late-O giants could also be slightly cooler objects as discussed in the previous paragraph.

A.3. Multiplicity

Sana et al. (2013) have determined from detailed radial-velocity analysis that 35% of the VFTS O stars are spectroscopic binaries with amplitudes greater than or equal to 20 km s^{-1} , corresponding to an intrinsic (bias-corrected) binary fraction of 51% for the orbital-period range considered ($P < 10^{3.5}$ days). They also detect an additional 11% with smaller amplitudes, some of which may have other physical origins, but all of which are characterized as “SB” in Tables 2 and A.1 here for simplicity, with the amplitude ranges specified. All of the SB designations here are from the work of Sana et al., except for the SB? (with displacements between stellar and nebular lines but no significant variations detected) which have been added here. In addition, visual multiples have been so designated from inspection of *HST*/WFC3 images here (but note that there was no WFC3 coverage at the time for some objects at the peripheries of the VFTS field). As specified in the notes to the tables, all of these categories sum to similar total multiplicity

rates of 140/213 or 66% for the AAA spectral types (Table 2), and 96/139 or 69% for the BBB (Table A.1). As already noted, most of the SB2 are in the BBB list, while the AAA SB are predominantly SB1. As also pointed out in the table notes, these percentages are lower limits because of the detectability gap between radial velocities and direct imaging, as well as unfavorable inclinations in the case of the former. The implications for astrophysical and population studies of O stars in the Magellanic Clouds and beyond are clear and should always be borne in mind.

Table A.1. BBB-Rated Spectral Classifications and Supporting Data for 139 VFTS O–B0 Stars

VFTS	SpT	Mult	AltID	Comment/ M_V
017	B0 V	SB1I
035	O9.5 III _n	SB2? VM2?
042	O9.5 III((n))	SB1I	...	Si iv weak, −4.7
047	O9 V + O9.5 V	SB2
049	O9.7 V: + B	SB2
051	OBpe	...	ST1-06	...
055	O8.5 V + O9.5 IV	SB2 VM2
056	O6.5 V + O6.5 V	SB2	ST1-07	H, He profiles triangular
058	O8.5: V + B	SB2	ST1-09	...
059	O9.5 III:	SB1	ST1-10	Si iv very weak, −3.8
061	ON8.5 III: + O9.7: V:	SB2
063	O5 III(n)(fc) + sec	SB2	ST1-11	...
066	O9.5 III(n)	SB1	...	Si iv very weak, −4.5
070	O9.7 II	SB?	...	Si iv very weak
077	O9.5: III _n	...	ST1-22	Si iv very weak, −3.4
080	O9.7 II-III((n))	...	ST1-23	Si iv weak, −4.2
097	B0 IV	SB?	ST1-31	...
102	O9: Vnnne+	...	ST1-32	Fe II emission; Dufton et al. 2011; runaway
104	O9.7 II-III((n))	Si iv very weak
105	O8: Vz + O9-B0	SB2 VM3	ST1-37	...
109	O9.7 II:n	...	ST1-38	He II λ 4686 emission wings, “Onfp”? Si iv very weak
113	O9.7 II or B0 IV ?	SBs	ST1-39	very sharp lines; He II broad; Si iv very weak
114	O8.5 IV + sec	SB2	ST1-41	...
116	O9.7: V: + B0: V:	SB2 VM2?	ST1-42	...
120	O9.5 IV:	SB2	ST1-43	...
125	Ope	SB2?	ST1-47	or n with He II emission; He I λ 4713 double
128	O9.5 III:((n))	...	ST1-49	Si iv weak, −3.3
131	O9.7
141	O9.5 II-III((n))	SB?	T88-6	Si iv very weak, −4.3; Walborn et al. 1999 B0.2 V
142	Op	...	ST1-58	composite: He II/He I λ 4541/ λ 4471 implies O6.5, but λ 4541/ λ 4387 & λ 4200/ λ 4144 O8.5; false Vz
145	O8fp	SB1s	T88-3	contaminated by Brey 73-1A; Walborn et al. 1999 O7-8 II
148	O9.7 II-III(n)	SB1 NC	...	Si iv very weak
150	O9.5 III	SB2	T88-4	“Onfp”? Si iv very weak, −4.6; Walborn et al. 1999 O9.5 V
151	O6.5 II(f)p	SBvs VM5	T88-2	composite: weak N iv & C iv emission, N v absorption; Walborn et al. 1999, 3 components: O4 III(f)p, O8 III, B1-2:p(e)
153	O9 III((n))	VM3	T88-5	Si iv weak, −5.0; Walborn et al. 1999 O7 V(z!) N strong
163	O8.5 IV	“(n)” but profiles triangular & variable
173	O9.7: II-III(n)p	SB1	ST1-73	“Onfp”; Si iv weak
174	O8 V + B0: V:	SB2	ST1-75	...
176	O6 V:(f) + O9.5: V:	SB2	ST1-77	...
183	B0 IV	SB?
187	O9 IV: + B0: V:	SB2	ST1-81	...
188	O9.7: III:	SB?	...	Si iv very weak, −4.0
192	O9.7 II or B0 IV ?	...	ST1-85	Si iv weak
201	O9.7 V + sec	SB2
205	O9.7 II((n)) or B0 IV((n)) ?	...	ST1-91	Si iv, C III very weak
207	O9.7 II((n))	...	ST1-92	Si iv, C III very weak
217	O4 V((fc)): + O5 V((fc)):	SB2	ST1-98	X-ray source

continued on next page

Table A.1. *continued*

VFTS	SpT	Mult	AltID	Comment/ M_V
226	O9.7 III	runaway; Si iv weak, -3.2
231	O9.7 IV:(n) + sec	SB2	ST1-103	...
241	B0 IV	Si iv weak
242	B0 IV	SB?	...	runaway, Si iv weak
253	O9.5 II	Si iv very weak, -4.6 ; H strong
304	O9.7 III	VM2?	...	Si iv weak; shallow WFC3 image appears extended, but deep symmetrical
310	O9.7 V:	contaminated by R135
313	B0 IV	Si iv weak
314	O9.7 IV:(n) + sec:	SB2
316	O9.7 V:	contaminated
318	O((n))p	SB1	...	composite: He lines imply O9.5 III; H δ B2 V from strong wings and no Si iv, C III; weak, narrow N iv emission, N v absorption present; -2.6
327	O8.5 V(n) + sec	SB2	P15	...
328	O9.5 III(n)	SB?	...	Si iv weak, -3.3 ; runaway
329	O9.7 II-III(n)	SB1	P19	Si iv weak
339	O9.5 IV(n)	...	P83	Si iv weak, -3.8
345	O9.7 III(n)	SB1	P103	Si iv very weak, -4.1
346	O9.7 III	...	P113	Si iv very weak, -3.6
347	B0 V	...	P116	-2.8
350	O8 V	SB2	P124	circular nebula, Rubio et al. 1998
352	O4.5 V(n)((fc)):z: + O5.5 V(n)((fc)):z:	SB2
360	O9.7	...	P169	Si iv strong; no He I $\lambda 4713$
370	O9.7 III	SB?	P222	Si iv weak, -3.4 ; runaway
371	O9.5 V(n) + sec	SB2	P240	...
373	O9.5n	...	P246	...
389	O9.5 IV	...	Mk58(E) P304	Si iv weak, -5.1 ; Walborn et al. 2002b O9.5 V; inadvertently “Mk58(w)” in Paper I
393	O9.5(n)	...	P324	...
400	O9.7	...	P348	...
405	O9.5:n
412	O9.7
443	O7: V(n): + O7: V(n):	SB2 VM2	P615	...
444	O9.7	SB?
445	O3-4 V:((fc)): + O4-7 V:((fc)):	SB2	P621	X-ray source
446	Onn((f))
450	O9.7 III: + O7::	SB2	Mk50 P643	I. Howarth et al., in prep.
451	O(n)	contaminated; bright circumstellar nebulosity
455	O5: V:n	SB11	P661	X-ray source
456	Onn	((fc))?
460	O7.5 V + O7.5 V	SB2	P674	...
464	O9.5:	VM2	P702	...
465	On	...	P700	...
475	O9.7 III	SB1	P722	Si iv weak, -4.5
476	O((n))
477	O((n))	contaminated? He I $\lambda 4713$ Oe?
487	O6.5: IV:((f)): + O6.5: IV:((f)):	SB2 VM2
492	O8 V + O9.5: V	SB2	Mk21 P830	...
495	O9.7 II-III n	...	P9019	Si iv very weak
496	B0 Vn	SB?	...	-3.8
497	O3.5 V((f))z + OB	...	R140d	contaminated

continued on next page

Table A.1. *continued*

VFTS	SpT	Mult	AltID	Comment/ M_V
500	O6.5 IV((fc)) + O6.5 V((fc))	SB2	...	X-ray source
514	O9.7 III	SB1	P9021	Si iv weak, -3.2
515	O8-9p	VM2	...	(subtract 513!) “Onfp”? variable? Si iv & C iii strong, He ii $\lambda 4686$ weak imply high luminosity
519	O3-4 ((f)) + OB + WN	SB1s	R140c	contaminated
522	O6 II-Iab(fc) + O5.5 V((fc)):	SB2
525	B0 Ia	SB	Mk38 P930	...
527	O6.5 Iafc + O6 Iaf	SB2	R139 P952	Taylor et al. 2011; X-ray source
528	O9.7(n)	...	P956	“Onfp”? Si iv very weak
529	O9.5(n)	SB?	P955	...
538	ON9 Ia: + O7.5: I:(f):	SB2 VM2	Mk22 P1024	...
539	O9.5(n)	...	P1012	...
540	B0 V	-3.8
543	O9 IV + O9.7: V	SB2	P1031	...
552	O8.5 III: + B	SB2
557	On	SB2
559	O9.7(n)	...	P1133	...
561	O9:(n)	SB1I	P1145	...
563	O9.7 III: + B0: V:	SB2 VM2	P1154	...
565	O9.5:	SB?
570	O9.5ne+	SB2	...	Fe ii emission
571	O9.5 II-III(n)	SB2?	...	Si iv weak
579	O9:((n))	SB? VM2	P1201	Knot 1; Walborn et al. 2002b O9.5 V; X-ray source
583	O8 V + O8.5 V	SB2
587	O9.7:	SB?
588	O9.5	SB1I	...	“Onfp”? Si iv weak
594	O9.7
607	O9.7 III	SB?	...	Si iv weak, -3.6
622	O9.7 III	SB?	...	Si iv weak
634	O V	VM2	P1473	z?
642	O5 Vz: + O8 Vz:	SB2
647	O8: V:
652	B2 Ip + O9 III:	SB2	Mk5 P1552	I. Howarth et al., in prep.
661	O6.5 V(n) + O9.7: V:	SB2	P1594	...
703	O7: V: + O8: V:	SB2	P1828	...
711	O9.7 III	...	P1850	Si iv very weak, -4.2
728	O9.7 II-III((n))	SB1	P1966	Si iv weak
733	O9.7p	SB1	P1988	“Onfp”; He ii wings; Si iv weak; N ii $\lambda 3995$ too strong
771	O9.7 III:(n)	SB2	P2104	...
774	O7.5 IVp + O8.5: V:	SB2 SB3?	...	He strong?
787	O9.7 III	SB	P2157	Si iv weak, -3.5
806	O5.5 V((fc)):z + O7 Vz:	SB2 NC	B1259	...
810	O9.7 V + B1: V:	SB2	P2242	...
859	O9.5 IV + sec	SB2
887	O9.5 II-IIIn	SB2 NC	...	Si iv very weak, -4.4

Notes. See Table 2 for explanation of notations in the Multiplicity and Alternate ID columns. 96/139 stars have multiplicity flags. The SB2 have been classified by JMA with MGB. There are 10 B0 stars, of which one is a supergiant. The “Si iv weak” spectra are further discussed in the text. Because of the very steep spectral-type dependence of the luminosity criteria at the O–B0 boundary, He ii $\lambda 4686$ /He i $\lambda 4713$ of or near unity implies class II at O9.7 but V–IV at B0; also, metallicity affects the sensitive Si iii $\lambda 4552$ /He ii $\lambda 4541$ spectral-type criterion, a value of or near unity defining type O9.7.